Measurement of the $B^0 \to \pi^- \ell^+ \nu$ and $B^+ \to \eta^{(\prime)} \ell^+ \nu$ branching fractions, the $B^0 \to \pi^- \ell^+ \nu$ and $B^+ \to \eta \ell^+ \nu$ form-factor shapes, and determination of $|V_{ub}|$

P. del Amo Sanchez,[1] J. P. Lees,[1] V. Poireau,[1] E. Prencipe,[1] V. Tisserand,[1] J. Garra Tico,[2] E. Grauges,[2] M. Martinelli,[3a,3b] D. A. Milanes,[3a,3b] A. Palano,[3a,3b] M. Pappagallo,[3a,3b] G. Eigen,[4] B. Stugu,[4] L. Sun,[4] D. N. Brown,[5] L. T. Kerth,[5] Yu. G. Kolomensky,[5] G. Lynch,[5] I. L. Osipenkov,[5] H. Koch,[6] T. Schroeder,[6] D. J. Asgeirsson,[7] C. Hearty,[7] T. S. Mattison,[7] J. A. McKenna,[7] A. Khan,[8] A. Randle-Conde,[8] V. E. Blinov,[9] A. R. Buzykaev,[9] V. P. Druzhinin,[9] V. B. Golubev,[9] E. A. Kravchenko,[9] A. P. Onuchin,[9] S. I. Serednyakov,[9] Yu. I. Skovpen,[9] E. P. Solodov,[9] K. Yu. Todyshev,[9] A. N. Yushkov,[9] M. Bondioli,[10] S. Curry,[10] D. Kirkby,[10] A. J. Lankford,[10] M. Mandelkern,[10] E. C. Martin,[10] D. P. Stoker,[10] H. Atmacan,[11] J. W. Gary,[11] F. Liu,[11] O. Long,[11] G. M. Vitug,[11] C. Campagnari,[12] T. M. Hong,[12] D. Kovalskyi,[12] J. D. Richman,[12] C. West,[12] A. M. Eisner,[13] C. A. Heusch,[13] J. Kroseberg,[13] W. S. Lockman,[13] A. J. Martinez,[13] T. Schalk,[13] B. A. Schumm,[13] A. Seiden,[13] L. O. Winstrom,[13] C. H. Cheng,[14] D. A. Doll,[14] B. Echenard,[14] D. G. Hitlin,[14] P. Ongmongkolkul,[14] F. C. Porter,[14] A. Y. Rakitin,[14] R. Andreassen,[15] M. S. Dubrovin,[15] G. Mancinelli,[15] B. T. Meadows,[15] M. D. Sokoloff,[15] P. C. Bloom,[16] W. T. Ford,[16] A. Gaz,[16] M. Nagel,[16] U. Nauenberg,[16] J. G. Smith,[16] S. R. Wagner,[16] R. Ayad,[17,*] W. H. Toki,[17] H. Jasper,[18] T. M. Karbach,[18] A. Petzold,[18] B. Spaan,[18] M. J. Kobel,[19] K. R. Schubert,[19] R. Schwierz,[19] D. Bernard,[20] M. Verderi,[20] P. J. Clark,[21] S. Playfer,[21] J. E. Watson,[21] M. Andreotti,[22a,22b] D. Bettoni,[22a] C. Bozzi,[22a] R. Calabrese,[22a,22b] A. Cecchi,[22a,22b] G. Cibinetto,[22a,22b] E. Fioravanti,[22a,22b] P. Franchini,[22a,22b] E. Luppi,[22a,22b] M. Munerato,[22a,22b] M. Negrini,[22a,22b] A. Petrella,[22a,22b] L. Piemontese,[22a] R. Baldini-Ferroli,[23] A. Calcaterra,[23] R. de Sangro,[23] G. Finocchiaro,[23] M. Nicolaci,[23] S. Pacetti,[23] P. Patteri,[23] I. M. Peruzzi,[23,†] M. Piccolo,[23] M. Rama,[23] A. Zallo,[23] R. Contri,[24a,24b] E. Guido,[24a,24b] M. Lo Vetere,[24a,24b] M. R. Monge,[24a,24b] S. Passaggio,[24a] C. Patrignani,[24a,24b] E. Robutti,[24a] S. Tosi,[24a,24b] B. Bhuyan,[25] V. Prasad,[25] C. L. Lee,[26] M. Morii,[26] A. Adametz,[27] J. Marks,[27] U. Uwer,[27] F. U. Bernlochner,[28] M. Ebert,[28] H. M. Lacker,[28] T. Lueck,[28] A. Volk,[28] P. D. Dauncey,[29] M. Tibbetts,[29] P. K. Behera,[30] U. Mallik,[30] C. Chen,[31] J. Cochran,[31] H. B. Crawley,[31] L. Dong,[31] W. T. Meyer,[31] S. Prell,[31] E. I. Rosenberg,[31] A. E. Rubin,[31] A. V. Gritsan,[32] Z. J. Guo,[32] N. Arnaud,[33] M. Davier,[33] D. Derkach,[33] J. Firmino da Costa,[33] G. Grosdidier,[33] F. Le Diberder,[33] A. M. Lutz,[33] B. Malaescu,[33] A. Perez,[33] P. Roudeau,[33] M. H. Schune,[33] J. Serrano,[33] V. Sordini,[33,‡] A. Stocchi,[33] L. Wang,[33] G. Wormser,[33] D. J. Lange,[34] D. M. Wright,[34] I. Bingham,[35] C. A. Chavez,[35] J. P. Coleman,[35] J. R. Fry,[35] E. Gabathuler,[35] R. Gamet,[35] D. E. Hutchcroft,[35] D. J. Payne,[35] C. Touramanis,[35] A. J. Bevan,[36] F. Di Lodovico,[36] R. Sacco,[36] M. Sigamani,[36] G. Cowan,[37] S. Paramesvaran,[37] A. C. Wren,[37] D. N. Brown,[38] C. L. Davis,[38] A. G. Denig,[39] M. Fritsch,[39] W. Gradl,[39] A. Hafner,[39] K. E. Alwyn,[40] D. Bailey,[40] R. J. Barlow,[40] G. Jackson,[40] G. D. Lafferty,[40] J. Anderson,[41] R. Cenci,[41] A. Jawahery,[41] D. A. Roberts,[41] G. Simi,[41] J. M. Tuggle,[41] C. Dallapiccola,[42] E. Salvati,[42] R. Cowan,[43] D. Dujmic,[43] G. Sciolla,[43] M. Zhao,[43] D. Lindemann,[44] P. M. Patel,[44] S. H. Robertson,[44] M. Schram,[44] P. Biassoni,[45a,45b] A. Lazzaro,[45a,45b] V. Lombardo,[45a] F. Palombo,[45a,45b] S. Stracka,[45a,45b] L. Cremaldi,[46] R. Godang,[46,§] R. Kroeger,[46] P. Sonnek,[46] D. J. Summers,[46] X. Nguyen,[47] M. Simard,[47] P. Taras,[47] G. De Nardo,[48a,48b] D. Monorchio,[48a,48b] G. Onorato,[48a,48b] C. Sciacca,[48a,48b] G. Raven,[49] H. L. Snoek,[49] C. P. Jessop,[50] K. J. Knoepfel,[50] J. M. LoSecco,[50] W. F. Wang,[50] L. A. Corwin,[51] K. Honscheid,[51] R. Kass,[51] J. P. Morris,[51] N. L. Blount,[52] J. Brau,[52] R. Frey,[52] O. Igonkina,[52] J. A. Kolb,[52] R. Rahmat,[52] N. B. Sinev,[52] D. Strom,[52] J. Strube,[52] E. Torrence,[52] G. Castelli,[53a,53b] E. Feltresi,[53a,53b] N. Gagliardi,[53a,53b] M. Margoni,[53a,53b] M. Morandin,[53a] M. Posocco,[53a] M. Rotondo,[53a] F. Simonetto,[53a,53b] R. Stroili,[53a,53b] E. Ben-Haim,[54] G. R. Bonneaud,[54] H. Briand,[54] G. Calderini,[54] J. Chauveau,[54] O. Hamon,[54] Ph. Leruste,[54] G. Marchiori,[54] J. Ocariz,[54] J. Prendki,[54] S. Sitt,[54] M. Biasini,[55a,55b] E. Manoni,[55a,55b] A. Rossi,[55a,55b] C. Angelini,[56a,56b] G. Batignani,[56a,56b] S. Bettarini,[56a,56b] M. Carpinelli,[56a,56b,‖] G. Casarosa,[56a,56b] A. Cervelli,[56a,56b] F. Forti,[56a,56b] M. A. Giorgi,[56a,56b] A. Lusiani,[56a,56c] N. Neri,[56a,56b] E. Paoloni,[56a,56b] G. Rizzo,[56a,56b] J. J. Walsh,[56a] D. Lopes Pegna,[57] C. Lu,[57] J. Olsen,[57] A. J. S. Smith,[57] A. V. Telnov,[57] F. Anulli,[58a] E. Baracchini,[58a,58b] G. Cavoto,[58a] R. Faccini,[58a,58b] F. Ferrarotto,[58a] F. Ferroni,[58a,58b] M. Gaspero,[58a,58b] L. Li Gioi,[58a] M. A. Mazzoni,[58a] G. Piredda,[58a] F. Renga,[58a,58b] T. Hartmann,[59] T. Leddig,[59] H. Schröder,[59] R. Waldi,[59] T. Adye,[60] B. Franek,[60] E. O. Olaiya,[60] F. F. Wilson,[60] S. Emery,[61] G. Hamel de Monchenault,[61] G. Vasseur,[61] Ch. Yèche,[61] M. Zito,[61] M. T. Allen,[62] D. Aston,[62] D. J. Bard,[62] R. Bartoldus,[62] J. F. Benitez,[62] C. Cartaro,[62] M. R. Convery,[62] J. Dorfan,[62] G. P. Dubois-Felsmann,[62] W. Dunwoodie,[62] R. C. Field,[62] M. Franco Sevilla,[62] B. G. Fulsom,[62] A. M. Gabareen,[62] M. T. Graham,[62] P. Grenier,[62] C. Hast,[62] W. R. Innes,[62] M. H. Kelsey,[62] H. Kim,[62] P. Kim,[62] M. L. Kocian,[62] D. W. G. S. Leith,[62] S. Li,[62] B. Lindquist,[62] S. Luitz,[62] H. L. Lynch,[62] D. B. MacFarlane,[62] H. Marsiske,[62] D. R. Muller,[62] H. Neal,[62] S. Nelson,[62] C. P. O'Grady,[62] I. Ofte,[62] M. Perl,[62] T. Pulliam,[62] B. N. Ratcliff,[62] A. Roodman,[62] A. A. Salnikov,[62] V. Santoro,[62] R. H. Schindler,[62] J. Schwiening,[62]

A. Snyder,[62] D. Su,[62] M. K. Sullivan,[62] S. Sun,[62] K. Suzuki,[62] J. M. Thompson,[62] J. Va'vra,[62] A. P. Wagner,[62] M. Weaver,[62] W. J. Wisniewski,[62] M. Wittgen,[62] D. H. Wright,[62] H. W. Wulsin,[62] A. K. Yarritu,[62] C. C. Young,[62] V. Ziegler,[62] X. R. Chen,[63] W. Park,[63] M. V. Purohit,[63] R. M. White,[63] J. R. Wilson,[63] S. J. Sekula,[64] M. Bellis,[65] P. R. Burchat,[65] A. J. Edwards,[65] T. S. Miyashita,[65] S. Ahmed,[66] M. S. Alam,[66] J. A. Ernst,[66] B. Pan,[66] M. A. Saeed,[66] S. B. Zain,[66] N. Guttman,[67] A. Soffer,[67] P. Lund,[68] S. M. Spanier,[68] R. Eckmann,[69] J. L. Ritchie,[69] A. M. Ruland,[69] C. J. Schilling,[69] R. F. Schwitters,[69] B. C. Wray,[69] J. M. Izen,[70] X. C. Lou,[70] F. Bianchi,[71a,71b] D. Gamba,[71a,71b] M. Pelliccioni,[71a,71b] M. Bomben,[72a,72b] L. Lanceri,[72a,72b] L. Vitale,[72a,72b] N. Lopez-March,[73] F. Martinez-Vidal,[73] A. Oyanguren,[73] J. Albert,[74] Sw. Banerjee,[74] H. H. F. Choi,[74] K. Hamano,[74] G. J. King,[74] R. Kowalewski,[74] M. J. Lewczuk,[74] C. Lindsay,[74] I. M. Nugent,[74] J. M. Roney,[74] R. J. Sobie,[74] T. J. Gershon,[75] P. F. Harrison,[75] T. E. Latham,[75] E. M. T. Puccio,[75] H. R. Band,[76] S. Dasu,[76] K. T. Flood,[76] Y. Pan,[76] R. Prepost,[76] C. O. Vuosalo,[76] and S. L. Wu[76]

(*BABAR* Collaboration)

[1]*Laboratoire d'Annecy-le-Vieux de Physique des Particules (LAPP), Université de Savoie, CNRS/IN2P3, F-74941 Annecy-Le-Vieux, France*
[2]*Universitat de Barcelona, Facultat de Fisica, Departament ECM, E-08028 Barcelona, Spain*
[3a]*INFN Sezione di Bari, I-70126 Bari, Italy*
[3b]*Dipartimento di Fisica, Università di Bari, I-70126 Bari, Italy*
[4]*University of Bergen, Institute of Physics, N-5007 Bergen, Norway*
[5]*Lawrence Berkeley National Laboratory and University of California, Berkeley, California 94720, USA*
[6]*Ruhr Universität Bochum, Institut für Experimentalphysik 1, D-44780 Bochum, Germany*
[7]*University of British Columbia, Vancouver, British Columbia, Canada V6T 1Z1*
[8]*Brunel University, Uxbridge, Middlesex UB8 3PH, United Kingdom*
[9]*Budker Institute of Nuclear Physics, Novosibirsk 630090, Russia*
[10]*University of California at Irvine, Irvine, California 92697, USA*
[11]*University of California at Riverside, Riverside, California 92521, USA*
[12]*University of California at Santa Barbara, Santa Barbara, California 93106, USA*
[13]*University of California at Santa Cruz, Institute for Particle Physics, Santa Cruz, California 95064, USA*
[14]*California Institute of Technology, Pasadena, California 91125, USA*
[15]*University of Cincinnati, Cincinnati, Ohio 45221, USA*
[16]*University of Colorado, Boulder, Colorado 80309, USA*
[17]*Colorado State University, Fort Collins, Colorado 80523, USA*
[18]*Technische Universität Dortmund, Fakultät Physik, D-44221 Dortmund, Germany*
[19]*Technische Universität Dresden, Institut für Kern- und Teilchenphysik, D-01062 Dresden, Germany*
[20]*Laboratoire Leprince-Ringuet, CNRS/IN2P3, Ecole Polytechnique, F-91128 Palaiseau, France*
[21]*University of Edinburgh, Edinburgh EH9 3JZ, United Kingdom*
[22a]*INFN Sezione di Ferrara, I-44100 Ferrara, Italy*
[22b]*Dipartimento di Fisica, Università di Ferrara, I-44100 Ferrara, Italy*
[23]*INFN Laboratori Nazionali di Frascati, I-00044 Frascati, Italy*
[24a]*INFN Sezione di Genova, I-16146 Genova, Italy*
[24b]*Dipartimento di Fisica, Università di Genova, I-16146 Genova, Italy*
[25]*Indian Institute of Technology Guwahati, Guwahati, Assam, 781 039, India*
[26]*Harvard University, Cambridge, Massachusetts 02138, USA*
[27]*Universität Heidelberg, Physikalisches Institut, Philosophenweg 12, D-69120 Heidelberg, Germany*
[28]*Humboldt-Universität zu Berlin, Institut für Physik, Newtonstraβe 15, D-12489 Berlin, Germany*
[29]*Imperial College London, London, SW7 2AZ, United Kingdom*
[30]*University of Iowa, Iowa City, Iowa 52242, USA*
[31]*Iowa State University, Ames, Iowa 50011-3160, USA*
[32]*Johns Hopkins University, Baltimore, Maryland 21218, USA*
[33]*Laboratoire de l'Accélérateur Linéaire, IN2P3/CNRS et Université Paris-Sud 11, Centre Scientifique d'Orsay, B. P. 34, F-91898 Orsay Cedex, France*
[34]*Lawrence Livermore National Laboratory, Livermore, California 94550, USA*
[35]*University of Liverpool, Liverpool L69 7ZE, United Kingdom*
[36]*Queen Mary, University of London, London, E1 4NS, United Kingdom*
[37]*University of London, Royal Holloway and Bedford New College, Egham, Surrey TW20 0EX, United Kingdom*
[38]*University of Louisville, Louisville, Kentucky 40292, USA*
[39]*Johannes Gutenberg-Universität Mainz, Institut für Kernphysik, D-55099 Mainz, Germany*
[40]*University of Manchester, Manchester M13 9PL, United Kingdom*

[41]*University of Maryland, College Park, Maryland 20742, USA*
[42]*University of Massachusetts, Amherst, Massachusetts 01003, USA*
[43]*Massachusetts Institute of Technology, Laboratory for Nuclear Science, Cambridge, Massachusetts 02139, USA*
[44]*McGill University, Montréal, Québec, Canada H3A 2T8*
[45a]*INFN Sezione di Milano, I-20133 Milano, Italy*
[45b]*Dipartimento di Fisica, Università di Milano, I-20133 Milano, Italy*
[46]*University of Mississippi, University, Mississippi 38677, USA*
[47]*Université de Montréal, Physique des Particules, Montréal, Québec, Canada H3C 3J7*
[48a]*INFN Sezione di Napoli, I-80126 Napoli, Italy*
[48b]*Dipartimento di Scienze Fisiche, Università di Napoli Federico II, I-80126 Napoli, Italy*
[49]*NIKHEF, National Institute for Nuclear Physics and High Energy Physics, NL-1009 DB Amsterdam, The Netherlands*
[50]*University of Notre Dame, Notre Dame, Indiana 46556, USA*
[51]*Ohio State University, Columbus, Ohio 43210, USA*
[52]*University of Oregon, Eugene, Oregon 97403, USA*
[53a]*INFN Sezione di Padova, I-35131 Padova, Italy*
[53b]*Dipartimento di Fisica, Università di Padova, I-35131 Padova, Italy*
[54]*Laboratoire de Physique Nucléaire et de Hautes Energies, IN2P3/CNRS, Université Pierre et Marie Curie-Paris6, Université Denis Diderot-Paris7, F-75252 Paris, France*
[55a]*INFN Sezione di Perugia, I-06100 Perugia, Italy*
[55b]*Dipartimento di Fisica, Università di Perugia, I-06100 Perugia, Italy*
[56a]*INFN Sezione di Pisa, I-56127 Pisa, Italy*
[56b]*Dipartimento di Fisica, Università di Pisa, I-56127 Pisa, Italy*
[56c]*Scuola Normale Superiore di Pisa, I-56127 Pisa, Italy*
[57]*Princeton University, Princeton, New Jersey 08544, USA*
[58a]*INFN Sezione di Roma, I-00185 Roma, Italy*
[58b]*Dipartimento di Fisica, Università di Roma La Sapienza, I-00185 Roma, Italy*
[59]*Universität Rostock, D-18051 Rostock, Germany*
[60]*Rutherford Appleton Laboratory, Chilton, Didcot, Oxon, OX11 0QX, United Kingdom*
[61]*CEA, Irfu, SPP, Centre de Saclay, F-91191 Gif-sur-Yvette, France*
[62]*SLAC National Accelerator Laboratory, Stanford, California 94309 USA*
[63]*University of South Carolina, Columbia, South Carolina 29208, USA*
[64]*Southern Methodist University, Dallas, Texas 75275, USA*
[65]*Stanford University, Stanford, California 94305-4060, USA*
[66]*State University of New York, Albany, New York 12222, USA*
[67]*Tel Aviv University, School of Physics and Astronomy, Tel Aviv, 69978, Israel*
[68]*University of Tennessee, Knoxville, Tennessee 37996, USA*
[69]*University of Texas at Austin, Austin, Texas 78712, USA*
[70]*University of Texas at Dallas, Richardson, Texas 75083, USA*
[71a]*INFN Sezione di Torino, I-10125 Torino, Italy*
[71b]*Dipartimento di Fisica Sperimentale, Università di Torino, I-10125 Torino, Italy*
[72a]*INFN Sezione di Trieste, I-34127 Trieste, Italy*
[72b]*Dipartimento di Fisica, Università di Trieste, I-34127 Trieste, Italy*
[73]*IFIC, Universitat de Valencia-CSIC, E-46071 Valencia, Spain*
[74]*University of Victoria, Victoria, British Columbia, Canada V8W 3P6*
[75]*Department of Physics, University of Warwick, Coventry CV4 7AL, United Kingdom*
[76]*University of Wisconsin, Madison, Wisconsin 53706, USA*

(Received 7 October 2010; published 24 March 2011)

We report the results of a study of the exclusive charmless semileptonic decays, $B^+ \to \eta^{(\prime)} \ell^+ \nu$ and $B^0 \to \pi^- \ell^+ \nu$, undertaken with approximately 464×10^6 $B\bar{B}$ pairs collected at the $\Upsilon(4S)$ resonance with the *BABAR* detector. The analysis uses events in which the signal B decays are reconstructed with a loose neutrino reconstruction technique. We obtain partial branching fractions for $B^+ \to \eta \ell^+ \nu$ and $B^0 \to \pi^- \ell^+ \nu$ decays in three and 12 bins of q^2, respectively, from which we extract the $f_+(q^2)$ form-factor shapes and the total branching fractions $\mathcal{B}(B^+ \to \eta \ell^+ \nu) = (0.36 \pm 0.05_{\rm stat} \pm 0.04_{\rm syst}) \times 10^{-4}$

[*]Now at Temple University, Philadelphia, PA 19122, USA.
[†]Also with Università di Perugia, Dipartimento di Fisica, Perugia, Italy.
[‡]Also with Università di Roma La Sapienza, I-00185 Roma, Italy.
[§]Now at University of South Alabama, Mobile, AL 36688, USA.
[‖]Also with Università di Sassari, Sassari, Italy.

and $\mathcal{B}(B^0 \to \pi^-\ell^+\nu) = (1.42 \pm 0.05_{\rm stat} \pm 0.07_{\rm syst}) \times 10^{-4}$. We also measure $\mathcal{B}(B^+ \to \eta'\ell^+\nu) = (0.24 \pm 0.08_{\rm stat} \pm 0.03_{\rm syst}) \times 10^{-4}$. We obtain values for the magnitude of the CKM matrix element $|V_{ub}|$ using three different QCD calculations.

DOI: 10.1103/PhysRevD.83.052011 PACS numbers: 13.20.He, 12.15.Hh, 12.38.Qk, 14.40.Nd

I. INTRODUCTION

A precise measurement of the CKM matrix [1] element $|V_{ub}|$ will constrain the description of weak interactions and CP violation in the standard model. The rate for exclusive charmless semileptonic decays involving a scalar meson is proportional to $|V_{ub}f_+(q^2)|^2$, where the form factor $f_+(q^2)$ depends on q^2, the square of the momentum transferred to the lepton-neutrino pair. Values of $f_+(q^2)$ are given by unquenched lattice QCD (LQCD) calculations [2,3], reliable only at large q^2 ($\gtrsim 16$ GeV^2), and by light cone sum rules (LCSR) calculations [4,5], based on approximations only valid at small q^2 ($\lesssim 16$ GeV^2). The value of $|V_{ub}|$ can thus be determined by the measurement of partial branching fractions of charmless semileptonic B decays. Extraction of the $f_+(q^2)$ form-factor shapes from exclusive decays [6] such as $B^0 \to \pi^-\ell^+\nu$ [7] and $B^+ \to \eta^{(\prime)}\ell^+\nu$ may be used to test theoretical calculations [8]. The values of the branching fractions (BF) of the $B^+ \to \eta^{(\prime)}\ell^+\nu$ decays will also improve our knowledge of the composition of charmless semileptonic decays and help constrain the size of the gluonic singlet contribution to the form factors for these decays [5].

In this paper, we present measurements of the partial BFs $\Delta\mathcal{B}(B^+ \to \eta\ell^+\nu, q^2)$ and $\Delta\mathcal{B}(B^0 \to \pi^-\ell^+\nu, q^2)$ in three and 12 bins of q^2, respectively, as well as the total BFs for all three decay modes. Values of the total BFs were previously reported in Refs. [7,9–12]. We use the values of $\Delta\mathcal{B}(q^2)$ for the $B^0 \to \pi^-\ell^+\nu$ mode with form-factor calculations [2–4] to obtain values of $|V_{ub}|$. Values of $|V_{ub}|$ have previously been extracted from $B^0 \to \pi^-\ell^+\nu$ measurements by CLEO [9], *BABAR* [7,10,13], and Belle [11]. A very recent measurement by *BABAR* [14] will be discussed in Sec. VII.

II. DATA SAMPLE AND SIMULATION

We use a sample of 464×10^6 $B\bar{B}$ pairs corresponding to an integrated luminosity of 422.6 fb^{-1} collected at the $\Upsilon(4S)$ resonance with the *BABAR* detector [15] at the PEP-II asymmetric-energy e^+e^- storage rings and a sample of 44 fb^{-1} collected approximately 40 MeV below the $\Upsilon(4S)$ resonance (denoted "off-resonance data"). Detailed Monte Carlo (MC) simulations are used to optimize the signal selections, to estimate the signal efficiencies, and to obtain the shapes of the signal and background distributions. MC samples are generated for $\Upsilon(4S) \to B\bar{B}$ events, $e^+e^- \to u\bar{u}/d\bar{d}/s\bar{s}/c\bar{c}/\tau^+\tau^-$ (continuum) events, and dedicated $B\bar{B}$ samples containing $B^0 \to \pi^-\ell^+\nu$ and $B^+ \to \eta^{(\prime)}\ell^+\nu$ signal decays. The signal MC events are produced with the FLATQ2 generator [16] and are reweighted to reproduce the $f_+(q^2, \alpha, c_B)$ Becirevic-Kaidalov (BK) parametrization [17], where the values of the shape and normalization parameters, α and c_B, are taken from Ref. [7]. The *BABAR* detector's acceptance and response are simulated using the GEANT4 package [15].

III. EVENT RECONSTRUCTION AND CANDIDATE SELECTION

We reconstruct the $B^0 \to \pi^-\ell^+\nu$ and $B^+ \to \eta^{(\prime)}\ell^+\nu$ decays. The η meson is reconstructed in the $\eta \to \gamma\gamma$ and $\eta \to \pi^+\pi^-\pi^0$ decay channels (combined BF of 62%) while the η' is reconstructed in the $\eta' \to \eta\pi^+\pi^-$ channel, followed by the $\eta \to \gamma\gamma$ decay (product BF of 17.5%) [18]. The $\eta' \to \rho^0\gamma$ decay channel suffers from large backgrounds, and we do not consider it. We carry out an untagged analysis with a loose neutrino reconstruction technique [7], thereby obtaining a large candidate sample.

Event reconstruction with the *BABAR* detector is described in detail elsewhere [15]. Electrons (muons) are identified by their characteristic shower signatures in the electromagnetic calorimeter (muon detector), while charged hadrons are identified using the Cherenkov detector and dE/dx measurements in the drift chamber. The average electron (muon) reconstruction efficiency is 93% (70%), while its misidentification probability is $<0.2\%$ ($< 1.5\%$). The neutrino four-momentum, $P_\nu = (|\vec{p}_{\rm miss}|, \vec{p}_{\rm miss})$, is inferred from the difference between the momentum of the colliding-beam particles $\vec{p}_{\rm beams}$ and the vector sum of the momenta of all the particles detected in a single event $\vec{p}_{\rm tot}$, such that $\vec{p}_{\rm miss} = \vec{p}_{\rm beams} - \vec{p}_{\rm tot}$. To evaluate $E_{\rm tot}$, the energy sum of all the particles, we assume zero mass for all neutrals since photons are difficult to disentangle from neutral hadrons, and we take the mass given by the particle identification selectors for the charged particles. In this analysis, we calculate the momentum transfer as $q^2 = (P_B - P_{\rm meson})^2$ instead of $q^2 = (P_\ell + P_\nu)^2$, where P_B, $P_{\rm meson}$, and P_ℓ are the four-momenta of the B meson, of the π, η, or η' meson, and of the lepton, respectively. With this choice, the value of q^2 is unaffected by any misreconstruction of the rest of the event. Here P_B has an effective value. To estimate this value, we first combine the lepton with a π, η, or η' meson to form the so-called Y pseudoparticle. The angle θ_{BY} between the Y and B momenta in the $\Upsilon(4S)$ frame can be determined by assuming $B \to Y\nu$. In this frame, the Y momentum, the B momentum, and the angle θ_{BY} define a cone with the Y momentum as its axis and where the true B momentum lies somewhere on the surface of the cone. The

B rest frame is thus known up to an azimuthal angle ϕ defined with respect to the Y momentum. The value of q^2 is then computed as the average of four q^2 values corresponding to four possible angles, ϕ, $\phi + \pi/2$, $\phi + \pi$, $\phi + 3\pi/2$ rad, where the angle ϕ is chosen randomly and where the four values of q^2 are weighted by the factor $\sin^2\theta_B$, θ_B being the angle between the B direction and the beam direction in the $\Upsilon(4S)$ frame [19]. We note that, θ_{BY} being a real angle, $|\cos\theta_{BY}| \leq 1$. We correct for the reconstruction effects on the q^2 resolution (0.51 GeV^2) by applying an unregularized unfolding algorithm to the measured q^2 spectra [20].

The candidate selections are optimized to maximize the ratio $S/\sqrt{(S+B)}$ in the MC simulation, where S is the number of signal events and B is the total number of background events. The continuum background is suppressed by requiring the ratio of second to zeroth Fox-Wolfram moments [21] to be smaller than 0.5. This background is further suppressed for $B^0 \to \pi^- \ell^+ \nu$ by selections on the number of charged particle tracks and neutral calorimeter clusters [22] that reject radiative Bhabha and converted photon processes. We ensure that the momenta of the lepton and meson candidates are kinematically compatible with a real signal decay by requiring that a geometrical vertex fit of the two particles gives a χ^2 probability greater than 0.01 and that their angles in the laboratory frame be between 0.41 and 2.46 rad with respect to the e^--beam direction, the acceptance of the detector. To avoid $J/\psi \to \mu^+\mu^-$ decays, we reject $B^0 \to \pi^- \mu^+ \nu$ candidates if the Y mass corresponds to the J/ψ mass. The electron (muon) tracks are required to have momenta greater than 0.5 (1.0) GeV in the laboratory frame to reduce misidentified leptons and secondary decays such as $D \to X\ell\nu$, J/ψ, τ, and kaon decays. Furthermore, the momenta of the lepton and the meson are restricted to enhance signal over background. We require the following: for $B^0 \to \pi^- \ell^+ \nu$ decays, $|\vec{p}^*_\ell| > 2.2$ GeV or $|\vec{p}^*_\pi| > 1.3$ GeV or $|\vec{p}^*_\ell| + |\vec{p}^*_\pi| > 2.8$ GeV; for $B^+ \to \eta \ell^+ \nu$ decays, $|\vec{p}^*_\ell| > 2.1$ GeV or $|\vec{p}^*_\eta| > 1.3$ GeV or $|\vec{p}^*_\ell| + |\vec{p}^*_\eta| > 2.8$ GeV; and for $B^+ \to \eta' \ell^+ \nu$ decays, $|\vec{p}^*_\ell| > 2.0$ GeV or $|\vec{p}^*_{\eta'}| > 1.65$ GeV or $0.69 \times |\vec{p}^*_\ell| + |\vec{p}^*_{\eta'}| > 2.4$ GeV (all asterisked variables are in the center-of-mass frame). For the $B^+ \to \eta^{(\prime)} \ell^+ \nu$ decays, we restrict the reconstructed masses of the η' and η to lie in the intervals $0.92 < m_{\eta'} < 0.98$ GeV and $0.51 < m_\eta < 0.57$ GeV. For these decays, we also reject events with q^2 higher than 16 GeV^2, since the signal is dominated by background in that range. Most backgrounds are reduced by q^2-dependent selections on the angle ($\cos\theta_{\rm thrust}$) between the thrust axes of the Y and of the rest of the event, on the polar angle ($\theta_{\rm miss}$) associated with $\vec{p}_{\rm miss}$, on the invariant missing mass squared ($m^2_{\rm miss} = E^2_{\rm miss} - |\vec{p}_{\rm miss}|^2$) divided by twice the missing energy ($E_{\rm miss} = E_{\rm beams} - E_{\rm tot}$), and on the angle ($\cos\theta_\ell$) between the direction of the W boson (ℓ and ν combined) in the rest frame of the B meson and the direction of the lepton in the rest frame of the W boson. The q^2 selections are shown in Fig. 1 and their effects illustrated in Fig. 2 for $B^0 \to \pi^- \ell^+ \nu$ decays. In Fig. 2, a single vertical line indicates a fixed cut; a set of two vertical lines represent a q^2-dependent cut. The position of the two lines corresponds to the minimum and maximum values of the cut, as shown in Fig. 1. The functions describing the q^2 dependence are given in Tables V, VI, and VII of the Appendix for the three decays under study. For $B^+ \to \eta \ell^+ \nu$ decays, more background is rejected by requiring that $|\cos\theta_V| < 0.95$, where θ_V is the helicity angle of the η meson [16].

The kinematic variables $\Delta E = (P_B \cdot P_{\rm beams} - s/2)/\sqrt{s}$ and $m_{ES} = \sqrt{(s/2 + \vec{p}_B \cdot \vec{p}_{\rm beams})^2/E^2_{\rm beams} - \vec{p}^{\,2}_B}$ are used in a two-dimensional extended maximum-likelihood fit [23] to separate signal from background. Here, $\sqrt{s}$ is the center-of-mass energy of the colliding particles and $P_B = P_{\rm meson} + P_\ell + P_\nu$, in the laboratory frame. We only retain candidates with $|\Delta E| < 1.0$ GeV and $m_{ES} > 5.19$ GeV, thereby removing the region with large backgrounds from the fit. On average, fewer than 1.14 candidates are observed per event. For events with multiple candidates, only the candidate with the largest value of $\cos\theta_\ell$ is kept. The signal event reconstruction efficiency varies between 8.3% and 14.6% for $B^0 \to \pi^- \ell^+ \nu$, and 1.4% and 2.6% for $B^+ \to \eta \ell^+ \nu$ decays ($\gamma\gamma$ channel), depending on q^2. It is 0.6% for both $B^+ \to \eta \ell^+ \nu$ ($\pi^+\pi^-\pi^0$ channel) and $B^+ \to \eta' \ell^+ \nu$ decays.

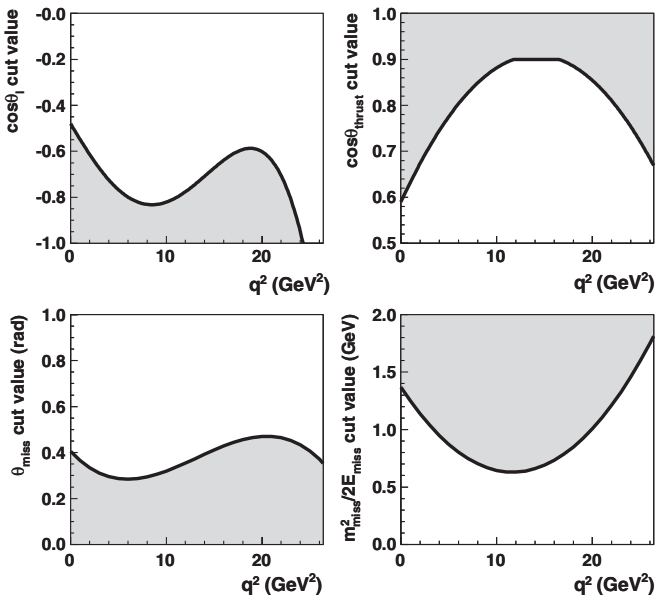

FIG. 1. Distributions of the selection values in the signal region for the q^2-dependent variables used in the analysis of $B^0 \to \pi^- \ell^+ \nu$ decays. The vertical axis represents the selection value for a given q^2 value. We reject an event when its value is in the shaded region.

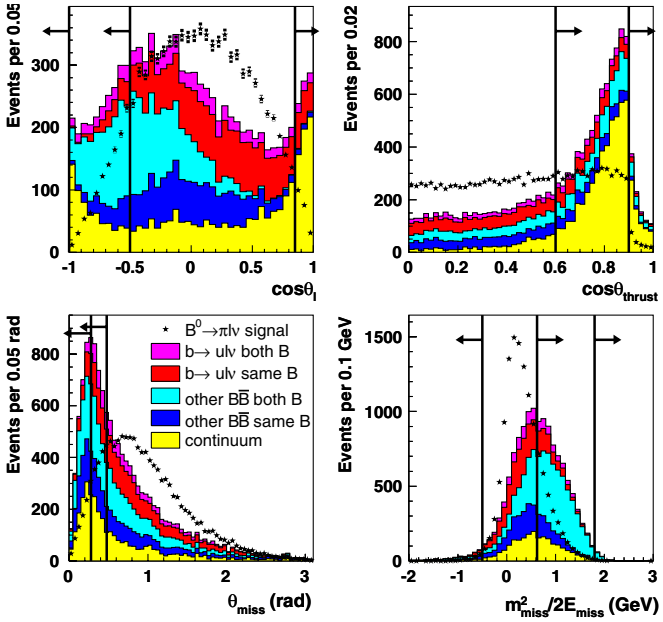

FIG. 2 (color online). Distributions in the signal region for the q^2-dependent selections used in the analysis of $B^0 \to \pi^- \ell^+ \nu$ decays. The arrows indicate the rejected regions. All the selections have been applied except for the one of interest. In each panel, the signal area is scaled to the area of the total background.

IV. BACKGROUNDS AND SIGNAL EXTRACTION

Backgrounds can be broadly grouped into three main categories: decays arising from $b \to u\ell\nu$ transitions (other than the signal), decays in other $B\bar{B}$ events (excluding $b \to u\ell\nu$), and decays in continuum events. For the $B^0 \to \pi^- \ell^+ \nu$ mode only, in which there are many events, each of the first two categories is further split into a background category where the pion and the lepton come from the decay of the same B, and a background category where the pion and the lepton come from the decay of different B mesons.

Given the sufficient number of events for the $\pi\ell\nu$ decay mode, the data samples can be subdivided into 12 bins of q^2 for the signal and two bins for each of the five background categories. Two bins are used for each background category since the background q^2 spectra are not that well known and need to be adjusted in the fit when the number of events is sufficiently large to permit it. The q^2 ranges of the background binning for the $B^0 \to \pi^- \ell^+ \nu$ decay are $[0, 18, 26.4]$ GeV^2 for the $b \to u\ell\nu$ same B category, $[0, 22, 26.4]$ GeV^2 for the $b \to u\ell\nu$ both B category, $[0, 10, 26.4]$ GeV^2 for the other $B\bar{B}$ same B category, $[0, 14, 26.4]$ GeV^2 for the other $B\bar{B}$ both B category and $[0, 22, 26.4]$ GeV^2 for the continuum category. In each case, the q^2 ranges of the two bins are chosen to contain a similar number of events. All the signal and background events, in each q^2 bin, are fitted simultaneously. For the $\eta^{(\prime)}\ell\nu$ modes, a smaller number of events leads us to restrict the signal and each of the three background categories to a single q^2 bin, except for the signal in the $\eta\ell\nu$ mode when $\eta \to \gamma\gamma$, which is investigated in three bins of q^2.

We use the ΔE-m_{ES} histograms, obtained from the MC simulation as two-dimensional probability density functions (PDFs), in our fit to the data to extract the yields of the signal and backgrounds as a function of q^2. As an initial estimate, the MC continuum background yield and q^2-dependent shape are first normalized to match the yield and q^2-dependent shape of the off-resonance data control sample. This results in a large statistical uncertainty due to the small number of events in the off-peak data. To improve the statistical precision, the continuum background, initially normalized to the off-peak data, is allowed to vary in the fit to the data for the $\pi\ell\nu$ and $\eta\ell\nu(\gamma\gamma)$ modes, where we have a large number of events. The fit result is compatible with the off-peak prediction within, at most, 1 standard deviation. Because of an insufficient number of events, the $b \to u\ell\nu$ background is fixed in the fit for the $\eta^{(\prime)}\ell\nu$ modes, and the continuum contribution is also fixed for the $\eta\ell\nu(3\pi)$ and $\eta'\ell\nu$ modes. Whenever a background is not varied in the fit, it is fixed to the MC prediction, except for the continuum background which is fixed to its normalized yield and q^2-dependent shape using the off-resonance data. The background parameters which are free in the fit require an adjustment of less than 10% with respect to the MC predictions. For illustration purposes only, we show in Fig. 3 ΔE and m_{ES} fit projections in the

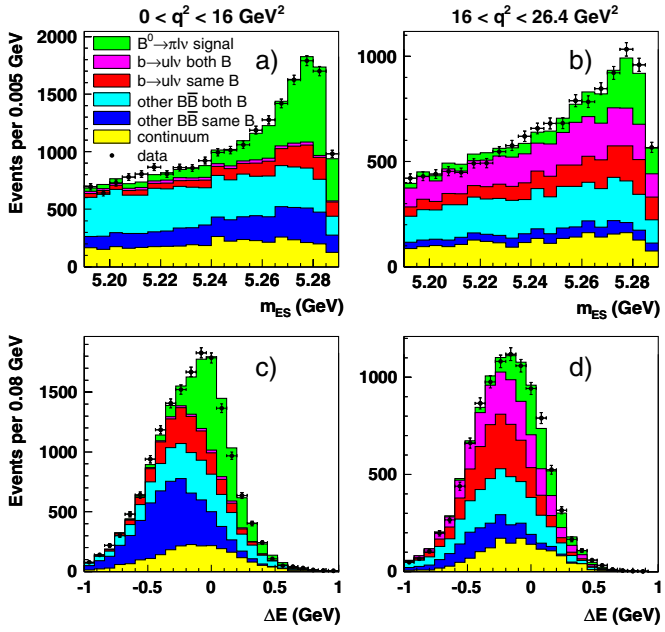

FIG. 3 (color online). Projections of the data and fit results for the $B^0 \to \pi^- \ell^+ \nu$ decays, in the signal-enhanced region: (a,b) m_{ES} with $-0.16 < \Delta E < 0.20$ GeV and (c,d) ΔE with $m_{ES} > 5.268$ GeV. The distributions (a,c) and (b,d) are projections for $q^2 < 16$ GeV^2 and for $q^2 > 16$ GeV^2, respectively.

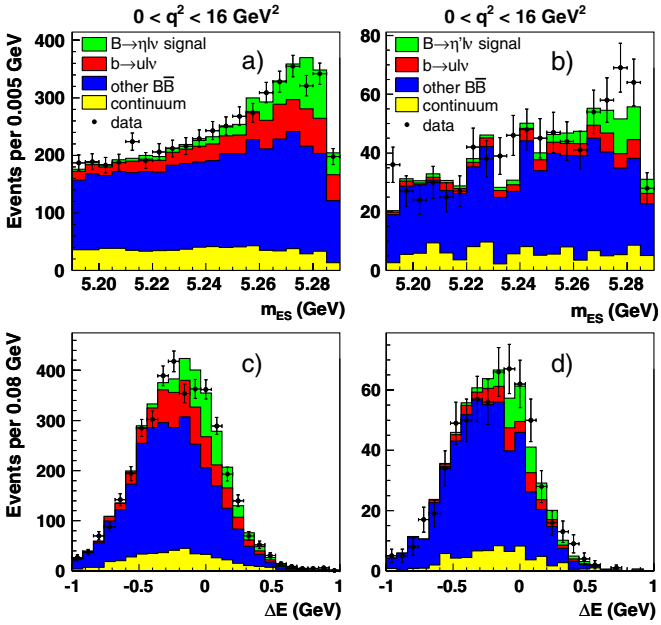

FIG. 4 (color online). Projections of the data and fit results for the $B^+ \to \eta^{(\prime)} \ell^+ \nu$ decays, in the signal-enhanced region: (a,b) m_{ES} with $-0.16 < \Delta E < 0.20$ GeV and (c,d) ΔE with $m_{ES} > 5.268$ GeV. The distributions (a,c) and (b,d) are projections for the $B^+ \to \eta \ell^+ \nu$ and $B^+ \to \eta' \ell^+ \nu$ decays, respectively, both for $q^2 < 16$ GeV^2.

signal-enhanced region for $B^0 \to \pi^- \ell^+ \nu$ decays in two ranges of q^2 corresponding to the sum of eight bins below and four bins above $q^2 = 16$ GeV^2, respectively. More detailed ΔE and m_{ES} fit projections in each q^2 bin are also shown in Figs. 8 and 9 of the Appendix for the $B^0 \to \pi^- \ell^+ \nu$ decays. The data and the fit results are in good agreement. Fit projections for $B^+ \to \eta^{(\prime)} \ell^+ \nu$, only available below $q^2 = 16$ GeV^2, are shown in Fig. 4. Table I gives the total fitted yields in the full q^2 range for the signal and each background category as well as the χ^2 values and degrees of freedom for the overall fit region. The yield values in the $B^+ \to \eta \ell^+ \nu$ column are the result of the fit to the combined $\gamma\gamma$ and 3π modes.

TABLE I. Fitted yields in the full q^2 range for the signal and each background category, total number of MC and data events, and values of χ^2 for the fit region.

Decay mode	$\pi^- \ell^+ \nu$	$\eta \ell^+ \nu$	$\eta' \ell^+ \nu$
Signal	11 778 ± 435	888 ± 98	141 ± 46
$b \to u \ell \nu$	27 793 ± 929	2201 (fixed)	204 (fixed)
Other $B\bar{B}$	80 185 ± 963	17 429 ± 247	2660 ± 82
Continuum	27 790 ± 814	3435 ± 195	517 (fixed)
MC events	147 546 ± 467	23 953 ± 183	3522 ± 68
Data events	147 529 ± 384	23 952 ± 155	3517 ± 59
χ^2/ndf	411/386	56/52	19/17

V. SYSTEMATIC UNCERTAINTIES

Systematic uncertainties on the values of the partial branching fractions, $\Delta\mathcal{B}(q^2)$, and their correlations among the q^2 bins have been investigated. These uncertainties are estimated from the variations of the resulting partial BF values (or total BF values for $B^+ \to \eta' \ell^+ \nu$ decays) when the data are reanalyzed with different simulation parameters and reweightings. For each parameter, we use the full MC data set to generate new ΔE-m_{ES} distributions (''MC event samples'') by varying randomly only the parameter of interest over a complete ($>3\sigma$) Gaussian distribution whose standard deviation is given by the uncertainty on the specific parameter under investigation. One hundred such samples are generated for each parameter. Uncertainties due to B counting and final state radiation are estimated by generating only one sample. Each MC sample is analyzed the same way as real data to determine values of $\Delta\mathcal{B}(q^2)$ (or total BF values for $B^+ \to \eta' \ell^+ \nu$ decays). The contribution of the parameter to the systematic uncertainty is given by the rms value of the distribution of these values over the 100 samples.

The systematic uncertainties due to the imperfect description of the detector in the simulation are computed by using the uncertainties, determined from control samples, on the tracking efficiency of all charged particle tracks, on the particle identification efficiencies of signal candidate tracks, on the calorimeter efficiencies (varied separately for photons and K_L^0), on the energy deposited in the calorimeter by K_L^0 mesons, as well as on their production spectrum. The reconstruction of these neutral particles affects the analysis through the neutrino reconstruction. The uncertainties due to the generator-level inputs to the simulation are given by the uncertainties in the BFs of the background processes $b \to u \ell \nu$ and $b \to c \ell \nu$, in the BFs of the secondary decays producing leptons [18], and in the BFs of the $\Upsilon(4S) \to B\bar{B}$ decays [8]. The $B \to X \ell \nu$ form-factor uncertainties, where $X = (\pi, \rho, \omega, \eta^{(\prime)}, D, D^*)$, are given by recent calculations or measurements [18]. The uncertainties in the heavy quark parameters used in the simulation of nonresonant $b \to u \ell \nu$ events are given in Ref. [24]. We assign an uncertainty of 20% [25] to the final state radiation (FSR) corrections calculated by PHOTOS [26]. Finally, the uncertainties due to the modeling of the continuum are established by using the uncertainty in its q^2 distribution shape and, when the continuum background is fixed, the uncertainty in the total yield, both given by comparisons with the off-resonance data control sample.

The list of all the systematic uncertainties, as well as their values for the partial and total BFs, are given in Tables VIII and IX of the Appendix. The item ''Signal MC stat error'' in these tables includes the systematic uncertainty due to the unfolding procedure. The correlation matrices obtained in the measurement of the partial BFs are presented in Tables X, XI, and XII. A condensed version of all the uncertainties is given in Table II together

TABLE II. Values of signal yields, $\Delta\mathcal{B}(q^2)$, and their relative uncertainties (%) for $B^0 \to \pi^-\ell^+\nu$, $B^+ \to \eta\ell^+\nu$, and $B^+ \to \eta'\ell^+\nu$ decays.

Decay mode	$\pi^-\ell^+\nu$				$\eta\ell^+\nu$	$\eta'\ell^+\nu$
q^2 range (GeV^2)	$q^2 < 12$	$q^2 < 16$	$q^2 > 16$	Full q^2 range	$q^2 < 16$	$q^2 < 16$
Yield	6541.6	8422.1	3355.4	11 777.6	887.9	141.0
BF (10^{-4})	0.83	1.09	0.33	1.42	0.36	0.24
Statistical error	3.9	3.7	7.6	3.5	12.5	32.8
Detector effects	3.1	3.5	6.1	4.0	8.0	8.8
Continuum bkg	0.9	0.8	1.0	0.7	0.3	7.1
$B \to X_u\ell\nu$ bkg	2.0	1.7	4.2	2.0	7.6	6.7
$B \to X_c\ell\nu$ bkg	0.6	0.7	1.8	1.0	1.2	2.6
Other effects	2.3	2.2	3.2	2.3	3.4	4.6
Total uncertainty	5.9	5.9	11.3	6.3	17.0	35.8

with signal yields and partial BFs in selected q^2 ranges. The values given for the $B^+ \to \eta\ell^+\nu$ decays are those obtained from the fits to the distributions of the $\eta \to \gamma\gamma$ and $\eta \to \pi^+\pi^-\pi^0$ channels combined. The larger relative uncertainties occurring in bin 12 of Table VIII are due to poorly reconstructed events, and to the small raw yield in that bin. The former arises from the presence of a large number of low momentum pions and a large background. This makes it difficult to select the right pion and results in a larger absolute uncertainty on the fitted yield. The small yield leads to a fairly large unfolding correction in this bin and thus to a considerably reduced unfolded yield. On the other hand, the unfolding process increases the absolute uncertainty only slightly. The reduced yield, together with the larger absolute uncertainty, leads to the larger relative uncertainties reported in the table.

VI. RESULTS

The partial BFs are calculated for $B^0 \to \pi^-\ell^+\nu$ and $B^+ \to \eta\ell^+\nu$ decays using the unfolded signal yields, the signal efficiencies given by the simulation, and the BFs $\mathcal{B}(\Upsilon(4S) \to B^0\bar{B}^0) = 0.484 \pm 0.006$ and $\mathcal{B}(\Upsilon(4S) \to B^+B^-) = 0.516 \pm 0.006$ [8]. We obtain the total BFs $\mathcal{B}(B^0 \to \pi^-\ell^+\nu) = (1.42 \pm 0.05_{\rm stat} \pm 0.07_{\rm syst}) \times 10^{-4}$, $\mathcal{B}(B^+ \to \eta\ell^+\nu) = (0.36 \pm 0.05_{\rm stat} \pm 0.04_{\rm syst}) \times 10^{-4}$, and $\mathcal{B}(B^+ \to \eta'\ell^+\nu) = (0.24 \pm 0.08_{\rm stat} \pm 0.03_{\rm syst}) \times 10^{-4}$. The BF value for $B^+ \to \eta'\ell^+\nu$ has a significance of 3.2σ when we take into account only the statistical uncertainty [27]. Taking into account the effect of the systematic uncertainty, which increases the total uncertainty by about 8%, leads to a reduced significance of 3.0σ. The BF value, obtained from a fit to the combined $\gamma\gamma$ and 3π channels of the $B^+ \to \eta\ell^+\nu$ decays, is in good agreement with the weighted average of the total BFs obtained separately for the $\gamma\gamma$ and 3π channels. Consistent results are obtained when dividing the final data set into chronologically ordered subsets, and electron only and muon only subsets, modifying the q^2 or the ΔE and m_{ES} binnings, and varying the event selection requirements.

The experimental $\Delta\mathcal{B}(q^2)$ distributions are displayed in Fig. 5 for $B^0 \to \pi^-\ell^+\nu$ decays and in Fig. 6 for $B^+ \to \eta\ell^+\nu$ decays, together with theoretical predictions. To allow a direct comparison with the theoretical predictions, which do not include FSR effects, the experimental distributions in these figures have been obtained with the efficiency given by the ratio of q^2 unfolded events generated after all the cuts, with a simulation which includes FSR, to the total number of events generated before any cut and with no FSR effects i.e. with PHOTOS switched off. We obtain the $f_+(q^2)$ shape from a fit to these distributions. The χ^2 function minimized in the fit to the $f_+(q^2)$ shape

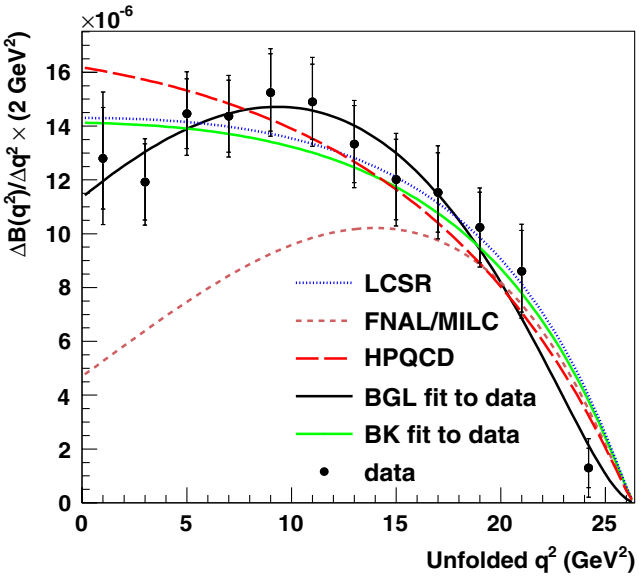

FIG. 5 (color online). Partial $\Delta\mathcal{B}(q^2)$ spectrum in 12 bins of q^2 for $B^0 \to \pi^-\ell^+\nu$ decays. The data points are placed in the middle of each bin whose width is defined in Table VIII. The smaller error bars are statistical only while the larger ones also include systematic uncertainties. The solid green and black curves show the result of the fit to the data of the BK [17] and BGL [28] parametrizations, respectively. The data are also compared to unquenched LQCD calculations (HPQCD [2], FNAL [3]) and a LCSR calculation [4].

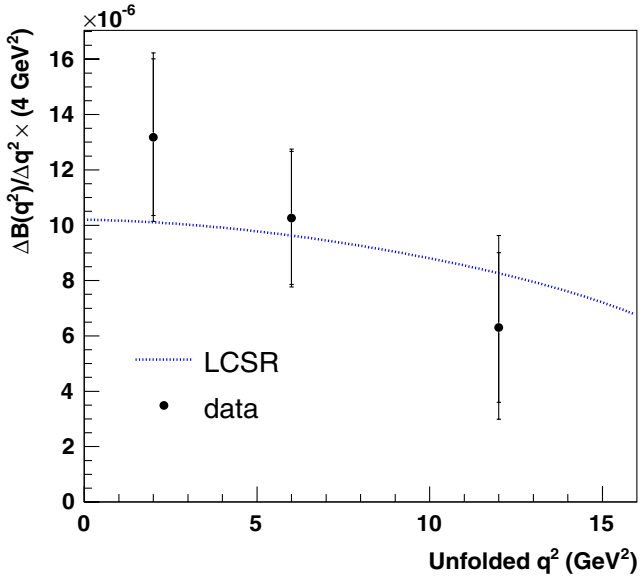

FIG. 6 (color online). Partial $\Delta\mathcal{B}(q^2)$ spectrum in three bins of q^2 for $B^+ \to \eta\ell^+\nu$ decays. The data points are placed in the middle of each bin whose width is defined in Table IX. The smaller error bars are statistical only while the larger ones also include systematic uncertainties. The data are also compared to a LCSR calculation [5].

uses the Boyd-Grinstein-Lebed (BGL) parametrization [28] consisting of a two-parameter polynomial expansion. For the $B^0 \to \pi^-\ell^+\nu$ decays, the fit gives $a_1/a_0 = -0.63 \pm 0.29$ and $a_2/a_0 = -6.9 \pm 1.7$, with $P(\chi^2) = 92.1\%$ as well as a value of $|V_{ub}f_+(0)| = (8.5 \pm 0.3_{\rm stat} \pm 0.2_{\rm syst}) \times 10^{-4}$ from the fit extrapolated to $q^2 = 0$. This value can be used to predict rates of other decays such as $B \to \pi\pi$ [29]. For completeness, we also show the fit to the BK parametrization [17], which gives $\alpha_{BK} = 0.52 \pm 0.04$, with $P(\chi^2) = 28.6\%$.

The q^2 distribution extracted from our data is compared in Fig. 5 to the shape of the form factors obtained from the three theoretical calculations listed in Table III: the one based on light cone sum rules [4] for $q^2 < 12$ GeV^2, and the two based on unquenched LQCD [2,3] for $q^2 > 16$ GeV^2. We first normalize the form-factor predictions to the experimental data by requiring the integrals of both to be the same over the q^2 ranges of validity given in Table III for each theoretical prediction. Considering only experimental uncertainties, we then calculate the χ^2 probabilities relative to the binned data result for various theoretical predictions. These are given in Table III for the $B^0 \to \pi^-\ell^+\nu$ decays. All three calculations are compatible with the data. As shown in Fig. 6, a LCSR calculation [5] is compatible with the data for the $B^+ \to \eta\ell^+\nu$ decays. It should be noted that the theoretical curves in Fig. 5 have been extrapolated over the full q^2 range based on a parametrization obtained over their q^2 ranges of validity. These extended ranges are only meant to illustrate a possible extension of the present theoretical calculations.

We extract a value of $|V_{ub}|$ from the $B^0 \to \pi^-\ell^+\nu$ $\Delta\mathcal{B}(q^2)$ distributions using the relation $|V_{ub}| = \sqrt{\Delta\mathcal{B}/(\tau_{B^0}\Delta\zeta)}$, where $\tau_{B^0} = 1.525 \pm 0.009$ ps [8] is the B^0 lifetime and $\Delta\zeta = \Gamma/|V_{ub}|^2$ is the normalized partial decay rate predicted by the form-factor calculations [2–4]. The quantities $\Delta\mathcal{B}$ and $\Delta\zeta$ are restricted to the q^2 ranges of validity given in Table III. The values of $\Delta\zeta$ are independent of experimental data. The values of $|V_{ub}|$ given in Table III range from $(3.1\text{–}3.7) \times 10^{-3}$. A value of $|V_{ub}|$ could not be obtained from the $B^+ \to \eta\ell^+\nu$ decays because the required theoretical input $\Delta\zeta$ is not yet available.

VII. COMBINED *BABAR* RESULTS

At first glance, there appears to be a large overlap between the present analysis of the $B^0 \to \pi^-\ell^+\nu$ data and that of another recent *BABAR* measurement [14]. However, there are significant differences between the two analyses. Considering the same fit region, we obtain 147 529 selected events (signal or background) compared to 42 516 such events in Ref. [14]. This difference can easily be explained by the fact that we use the full *BABAR* data set in the present analysis, but this is not so in Ref. [14]. Furthermore, the use of the loose neutrino reconstruction technique in this work leads to a larger background. Only 140 events are found in common between the two data sets, i.e. 0.3% overlap. The statistical uncertainties are thus expected to be uncorrelated between the two analyses. The event reconstruction and simulation are also somewhat different. For example, the values of q^2 are computed using different, although in principle equivalent, relations: here, $q^2 = (P_B - P_\pi)^2$ versus $q^2 = (P_\ell + P_\nu)^2$ in Ref. [14]. Nevertheless, almost all of the systematic uncertainties are expected to be highly correlated.

TABLE III. Values of $|V_{ub}|$ derived from the form-factor calculations for the $B^0 \to \pi^-\ell^+\nu$ decays. The three uncertainties on $|V_{ub}|$ are statistical, systematic, and theoretical, respectively.

	q^2 (GeV^2)	$\Delta\mathcal{B}$ (10^{-4})	$\Delta\zeta$ (ps^{-1})	$\lvert V_{ub}\rvert$ (10^{-3})	χ^2/ndf	Probability (χ^2)
HPQCD [2]	>16	$0.33 \pm 0.03 \pm 0.03$	2.02 ± 0.55	$3.28 \pm 0.13 \pm 0.15^{+0.57}_{-0.37}$	5.0/4	28.8%
FNAL [3]	>16	$0.33 \pm 0.03 \pm 0.03$	$2.21^{+0.47}_{-0.42}$	$3.14 \pm 0.12 \pm 0.14^{+0.35}_{-0.29}$	6.4/4	17.4%
LCSR [4]	<12	$0.84 \pm 0.03 \pm 0.04$	$4.00^{+1.01}_{-0.95}$	$3.70 \pm 0.07 \pm 0.08^{+0.54}_{-0.39}$	6.2/6	39.9%

TABLE IV. Values of quantities of interest and their averages obtained in the study of $B^0 \to \pi^- \ell^+ \nu$ decays. The third uncertainty, given for the average values, is due to the form-factor calculation. It is not shown for the individual determination of $|V_{ub}|$. The results for a_1/a_0, a_2/a_0, and $|V_{ub} f_+(0)|$ in the column titled "Average" are actually from a fit to the combined data, as discussed in the text.

	Present work	Reference [14]	Average
Total BF	$1.42 \pm 0.05 \pm 0.07$	$1.41 \pm 0.05 \pm 0.07$	$1.42 \pm 0.04 \pm 0.07$
$\|V_{ub}\|_{\mathrm{HPQCD}} \times 10^3$	$3.28 \pm 0.13 \pm 0.15$	$3.21 \pm 0.13 \pm 0.12$	$3.23 \pm 0.09 \pm 0.13^{+0.57}_{-0.37}$
$\|V_{ub}\|_{\mathrm{FNAL}} \times 10^3$	$3.14 \pm 0.12 \pm 0.14$	$3.07 \pm 0.11 \pm 0.11$	$3.09 \pm 0.08 \pm 0.12^{+0.35}_{-0.29}$
$\|V_{ub}\|_{\mathrm{LCSR}} \times 10^3$	$3.70 \pm 0.07 \pm 0.08$	$3.78 \pm 0.08 \pm 0.10$	$3.72 \pm 0.05 \pm 0.09^{+0.54}_{-0.39}$
$\|V_{ub} f_+(0)\| \times 10^4$	$8.5 \pm 0.3 \pm 0.2$	$10.8 \pm 0.5 \pm 0.3$	$9.4 \pm 0.3 \pm 0.3$
BGL a_1/a_0	$-0.63 \pm 0.27 \pm 0.10$	$-0.82 \pm 0.23 \pm 0.17$	$-0.79 \pm 0.14 \pm 0.14$
BGL a_2/a_0	$-6.9 \pm 1.3 \pm 1.1$	$-1.1 \pm 1.6 \pm 0.9$	$-4.4 \pm 0.8 \pm 0.9$

It is gratifying to note that, as shown in Table IV, the total BF as well as the values of $|V_{ub}|$ obtained in the two analyses are in good agreement with each other. The value of $|V_{ub}|$ quoted under Ref. [14] in Table IV for the FNAL [3] theoretical prediction is obtained using the values of the partial BFs given in Ref. [14] for $q^2 > 16$ GeV^2. Similar numbers of signal events ($11\,778 \pm 435$ here compared with $10\,604 \pm 376$ in Ref. [14] when the events from $B^+ \to \pi^0 \ell^+ \nu$ decays are also included) lead to similar statistical uncertainties in the two analyses.

It is possible to obtain a good approximation to the average of the present results and those of Ref. [14] obtained in the $B^0 \to \pi^- \ell^+ \nu$ decays by taking the statistical uncertainties to be uncorrelated and the systematic uncertainties to be fully correlated. The additional $|V_{ub}|$ value obtained in Ref. [14] with a combined fit to data and theoretical points is not included in the average values given in Table IV. We employ the above averaging procedure to determine the averages, and associated uncertainties, given in Table IV for the total branching fraction and the values of $|V_{ub}|$.

This averaging method is not appropriate for the fitted BGL coefficients (a_1/a_0 and a_2/a_0) and the value of $|V_{ub} f_+(0)|$, since, as shown in Table IV, the two measurements of these quantities are only marginally compatible. Instead, we perform a new fit of the BGL parametrization to the combined partial branching fraction results from the two analyses, the 12 values obtained in this analysis and the six values from Ref. [14]. Here again, the statistical covariance matrices are uncorrelated and the systematic covariance matrices are fully correlated between the two data sets. The combined error matrix from the two analyses is used to perform the fit, with the result shown in Fig. 7 and a χ^2 probability $P(\chi^2) = 14.2\%$. When only the statistical covariance matrix is used, the χ^2 probability is reduced to 3.1%. We note that the discrepancy in the two analyses of the partial BFs at low values of q^2 does not lead to discrepancies in the resulting values of the total BF or $|V_{ub}|$, as is evident in Table IV. Finally, we do not attempt to average the partial branching fractions due to the different q^2 binning used in the two analyses.

VIII. SUMMARY

In summary, we have measured the partial BFs of $B^+ \to \eta \ell^+ \nu$ decays in three bins of q^2 and of $B^0 \to \pi^- \ell^+ \nu$ decays in 12 bins of q^2. From these distributions, we extract the $f_+(q^2)$ shapes which are found to be compatible with all three theoretical predictions considered for the $B^0 \to \pi^- \ell^+ \nu$ decays and with the LCSR calculation for the $B^+ \to \eta \ell^+ \nu$ decays. The BGL parametrization fits our data well and allows us to obtain the value of $|V_{ub} f_+(0)|$. Our measured branching fractions of the three decays reported in this work lead to a significant improvement in our knowledge of the composition of the inclusive charmless semileptonic decay rate. Our value of the total BF for $B^+ \to \eta' \ell^+ \nu$ is an order of magnitude smaller than the most recent CLEO result [9]. Our value

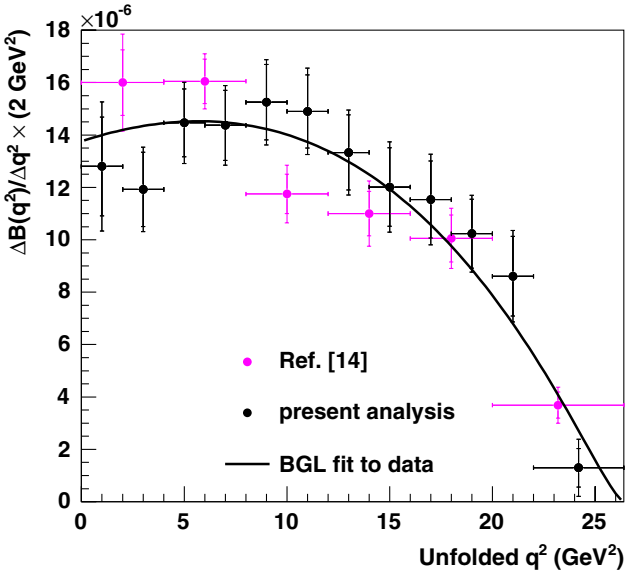

FIG. 7 (color online). Partial $\Delta\mathcal{B}(q^2)$ spectrum for $B^0 \to \pi^- \ell^+ \nu$ decays, in 12 bins of q^2 for the present work and six bins of q^2 for Ref. [14]. The smaller error bars are statistical only while the larger ones also include systematic uncertainties. The solid black curve shows the result of the fit to the combined data for the two analyses using the BGL [28] parametrization.

of the total BF for $B^+ \to \eta \ell^+ \nu$ is consistent with a previous untagged *BABAR* result [12]. The value of the ratio $\mathcal{B}(B^+ \to \eta' \ell^+ \nu)/\mathcal{B}(B^+ \to \eta \ell^+ \nu) = 0.67 \pm 0.24_{\text{stat}} \pm 0.11_{\text{syst}}$ allows an important gluonic singlet contribution to the η' form factor. The present value of the total BF for $B^0 \to \pi^- \ell^+ \nu$ is in good agreement with a previous untagged *BABAR* measurement [7] as well as with a recent *BABAR* result [14]. It has comparable precision to the present world average [8]. For $B^0 \to \pi^- \ell^+ \nu$ decays, we obtain values of $|V_{ub}|$ for three different QCD calculations. The results are in good agreement with those of Refs. [7,14]. The three values are all acceptable according to the data. Two of these values [2,4] are consistent, within large theoretical uncertainties, with the value measured in inclusive semileptonic B decays: $|V_{ub}| = (4.27 \pm 0.38) \times 10^{-3}$ [8]. We also provide the average values of the total BF and of $|V_{ub}|$ obtained in the present work and those of Ref. [14]. We also give the values of $|V_{ub} f_+(0)|$, a_1/a_0, and a_2/a_0 obtained in a combined BGL fit to the two data sets. It may be noted that our results for the $B^0 \to \pi^- \ell^+ \nu$ decays are generally in good agreement with those obtained recently by the Belle Collaboration [30].

ACKNOWLEDGMENTS

We would like to thank A. Khodjamirian, A. Kronfeld, and R. Van de Water for useful discussions concerning their form-factor calculations and for providing the values of $\Delta\zeta$ used in this work. We would also like to thank J. Dingfelder and B. Viaud for their numerous contributions to this analysis. We are grateful for the extraordinary contributions of our PEP-II colleagues in achieving the excellent luminosity and machine conditions that have made this work possible. The success of this project also relies critically on the expertise and dedication of the computing organizations that support *BABAR*. The collaborating institutions wish to thank SLAC for its support and the kind hospitality extended to them. This work is supported by the U.S. Department of Energy and National Science Foundation, the Natural Sciences and Engineering Research Council (Canada), the Commissariat à l'Energie Atomique and Institut National de Physique Nucléaire et de Physique des Particules (France), the Bundesministerium für Bildung und Forschung and Deutsche Forschungsgemeinschaft (Germany), the Istituto Nazionale di Fisica Nucleare (Italy), the Foundation for Fundamental Research on Matter (The Netherlands), the Research Council of Norway, the Ministry of Education and Science of the Russian Federation, Ministerio de Ciencia e Innovación (Spain), and the Science and Technology Facilities Council (United Kingdom). Individuals have received support from the Marie-Curie IEF program (European Union), the A. P. Sloan Foundation (U.S.) and the Binational Science Foundation (U.S.-Israel).

APPENDIX

In Tables V, VI, and VII, we give the functions describing the q^2 dependence of the selections used to reduce the backgrounds in the three decays under study.

The list of all the systematic uncertainties, as well as their values for the partial and total BFs, are given in Tables VIII and IX for the $B^0 \to \pi^- \ell^+ \nu$ and $B^+ \to \eta^{(\prime)} \ell^+ \nu$ decays, respectively. In Table VIII, we have one column for each bin

TABLE V. q^2-dependent selections used in $B^0 \to \pi^- \ell^+ \nu$ decays.

$\cos\theta_\ell < 0.85$ for all values of q^2
$\cos\theta_\ell > -0.000\,016\,7 * q^8 + 0.000\,462 * q^6 + 0.000\,656 * q^4 - 0.0701 * q^2 - 0.48$
$m^2_{\text{miss}}/2E_{\text{miss}} > -0.5$ GeV for all values of q^2
$m^2_{\text{miss}}/2E_{\text{miss}} < 0.005\,44 * q^4 - 0.127 * q^2 + 1.37$ GeV
$\cos\theta_{\text{thrust}} < 0.9$ for all values of q^2
$\cos\theta_{\text{thrust}} < -0.001\,59 * q^4 + 0.0451 * q^2 + 0.59$
$\theta_{\text{miss}} > -0.000\,122 * q^6 + 0.004\,83 * q^4 - 0.0446 * q^2 + 0.405$ rad
(q^2 is given in units of GeV^2)

TABLE VI. q^2-dependent selections used in $B^+ \to \eta \ell^+ \nu$ decays.

$\cos\theta_\ell < 0.9$ for all values of q^2
$\cos\theta_\ell > 0.00629 * q^4 - 0.119 * q^2 - 0.252$
$m^2_{\text{miss}}/2E_{\text{miss}} < 0.8$ GeV, $q^2 < 7.5$ GeV^2
$m^2_{\text{miss}}/2E_{\text{miss}} < -0.05 * q^2 + 1.175$ GeV, $7.5 < q^2 < 16.0$ GeV^2
$\cos\theta_{\text{thrust}} < 0.05 * q^2 + 0.6$, $q^2 < 5.0$ GeV^2
$\cos\theta_{\text{thrust}} < 0.85$, $5.0 < q^2 < 16.0$ GeV^2
$\cos\theta_{\text{miss}} < 0.92$, $q^2 < 11.0$ GeV^2
$\cos\theta_{\text{miss}} < 0.88$, $11.0 < q^2 < 16.0$ GeV^2
(q^2 is given in units of GeV^2)

TABLE VII. q^2-dependent selections used in $B^+ \to \eta' \ell^+ \nu$ decays.

$m^2_{\text{miss}}/2E_{\text{miss}} > -0.3$ GeV for all values of q^2
$m^2_{\text{miss}}/2E_{\text{miss}} < 0.35 * q^2 + 0.325$ GeV, $q^2 < 2.5$ GeV^2
$m^2_{\text{miss}}/2E_{\text{miss}} < 1.2$ GeV, $2.5 < q^2 < 4.5$ GeV^2
$m^2_{\text{miss}}/2E_{\text{miss}} < -0.1 * q^2 + 1.65$ GeV, $q^2 > 4.5$ GeV^2
$\cos\theta_{\text{thrust}} < 0.05 * q^2 + 0.575$, $q^2 < 6.5$ GeV^2
$\cos\theta_{\text{thrust}} < 0.9$, $6.5 < q^2 < 12.5$ GeV^2
$\cos\theta_{\text{thrust}} < -0.05 * q^2 + 1.525$, $q^2 > 12.5$ GeV^2
$\theta_{\text{miss}} > -0.1 * q^2 + 0.45$ rad, $q^2 < 2.5$GeV^2
$\theta_{\text{miss}} > 0.2$ rad, $2.5 < q^2 < 5.5$ GeV^2
$\theta_{\text{miss}} > 0.05 * q^2 - 0.075$ rad, $q^2 > 5.5$ GeV^2
(q^2 is given in units of GeV^2)

TABLE VIII. $B^0 \to \pi^- \ell^+ \nu$ yields, efficiencies (%), $\Delta\mathcal{B}$ (10^{-7}), and their relative uncertainties (%). The $\Delta\mathcal{B}$ and efficiency values labeled "without FSR" are modified to remove FSR effects. This procedure has no significant impact on the $\Delta\mathcal{B}$ values.

q^2 bins (GeV^2)	0–2	2–4	4–6	6–8	8–10	10–12	12–14	14–16	16–18	18–20	20–22	22–26.4	$q^2 < 12$	$q^2 < 16$	$q^2 > 16$	Total
Fitted yield	894.7	987.8	1177.1	1181.3	1178.6	1122.1	996.1	884.5	904.3	847.5	729.9	873.9	6541.6	8422.1	3355.4	11777.6
Yield statistical error	12.8	8.1	6.0	6.4	6.7	7.0	8.2	9.8	10.3	10.5	14.0	21.0	3.2	3.6	7.9	3.7
Efficiency	8.34	9.10	9.22	9.09	8.59	8.46	8.53	8.50	9.40	10.52	11.61	14.59	...	...	...	...
Efficiency (without FSR)	8.00	8.97	9.15	9.18	8.63	8.53	8.58	8.61	9.45	10.66	11.71	14.70	...	...	...	...
Unfolded yield	919.9	960.7	1189.6	1184.5	1182.9	1141.5	1027.3	929.2	979.5	979.9	905.8	376.7	6579.1	8535.7	3241.9	11777.6
$\Delta\mathcal{B}$	122.7	117.6	143.6	145.0	153.4	150.2	134.1	121.7	116.0	103.7	86.8	28.7	832.5	1088.3	335.3	1423.5
$\Delta\mathcal{B}$ (without FSR)	128.0	119.2	144.6	143.7	152.5	149.0	133.3	120.1	115.3	102.3	86.1	28.5	837.1	1090.5	332.3	1422.8
Tracking efficiency	3.2	1.9	3.1	2.2	2.3	3.9	2.6	4.0	3.5	1.3	4.1	9.4	2.3	2.5	2.9	2.6
Photon efficiency	6.0	3.4	2.6	1.3	2.2	2.5	3.1	3.0	5.0	1.4	5.1	24.2	1.9	2.2	4.6	2.7
K_L^0 efficiency	0.9	0.3	0.6	0.3	0.5	0.4	0.5	0.8	0.6	0.4	1.7	6.8	0.3	0.3	1.0	0.4
K_L^0 production spectrum	1.0	0.6	1.0	0.6	1.1	1.0	0.6	2.7	1.7	1.0	2.0	8.3	0.7	0.9	1.9	1.1
K_L^0 energy	1.0	0.6	0.3	0.2	0.2	0.3	0.2	0.4	0.6	0.7	0.8	7.1	0.2	0.3	0.8	0.3
ℓ identification	4.0	1.0	1.2	1.3	0.6	0.6	1.6	1.0	0.9	1.6	0.7	4.9	0.3	0.5	1.1	0.6
π identification	0.5	0.2	0.2	0.2	0.2	0.2	0.2	0.3	0.3	0.3	0.3	5.5	0.2	0.2	0.7	0.3
Bremsstrahlung	0.6	0.3	0.1	0.2	0.2	0.2	0.2	0.3	0.3	0.3	0.3	5.3	0.2	0.2	0.7	0.3
q^2 continuum shape	7.9	1.6	0.9	0.3	0.7	0.3	1.1	0.3	0.7	1.1	1.2	5.4	0.9	0.8	1.0	0.7
$\mathcal{B}(B^+ \to \pi^0 \ell^+ \nu)$	0.5	0.1	0.1	0.1	0.1	0.1	0.2	0.3	0.3	0.3	0.4	7.1	0.2	0.2	0.8	0.3
$\mathcal{B}(B^0 \to \rho^- \ell^+ \nu)$	0.5	0.3	0.1	0.1	0.2	0.1	0.2	0.3	0.3	0.3	0.5	10.1	0.2	0.2	0.9	0.3
$\mathcal{B}(B^+ \to \rho^0 \ell^+ \nu)$	0.7	0.2	0.1	0.1	0.2	0.2	0.2	0.3	0.4	0.3	0.3	7.3	0.2	0.2	0.8	0.3
$\mathcal{B}(B^+ \to \omega \ell^+ \nu)$	0.5	0.1	0.1	0.1	0.1	0.1	0.2	0.3	0.3	0.4	0.3	8.2	0.2	0.2	0.9	0.3
$\mathcal{B}(B^+ \to \eta \ell^+ \nu)$	0.5	0.1	0.1	0.1	0.1	0.1	0.2	0.3	0.3	0.3	0.2	5.5	0.2	0.2	0.7	0.3
$\mathcal{B}(B^+ \to \eta' \ell^+ \nu)$	0.5	0.1	0.1	0.1	0.1	0.1	0.2	0.3	0.3	0.3	0.3	5.4	0.2	0.2	0.7	0.3
Nonresonant $b \to u \ell \nu$ BF	0.6	0.3	0.1	0.1	0.2	0.2	0.2	0.4	0.5	0.3	0.6	7.8	0.2	0.2	0.7	0.3
SF parameters	0.9	0.5	0.9	0.4	0.3	0.5	0.6	0.3	0.5	2.3	4.1	23.4	0.6	0.4	2.3	0.8
$B \to \rho \ell \nu$ FF	2.4	1.4	2.1	1.4	1.9	1.6	0.8	0.7	2.4	3.0	1.1	16.6	1.8	1.5	1.8	1.5
$B^0 \to \pi^- \ell^+ \nu$ FF	0.5	0.1	0.1	0.1	0.1	0.1	0.2	0.3	0.3	0.3	0.3	7.5	0.2	0.2	0.9	0.3
Other scalar FF	1.1	0.3	0.5	0.5	0.4	0.3	0.3	0.7	1.7	2.1	2.0	8.7	0.4	0.3	0.6	0.3
$B \to \omega \ell \nu$ FF	0.6	0.1	0.1	0.1	0.1	0.1	0.2	0.3	0.5	0.6	0.6	18.1	0.2	0.2	1.8	0.5
$\mathcal{B}(B \to D \ell \nu)$	0.6	0.6	0.2	0.1	0.3	0.2	0.5	0.3	0.4	0.4	0.4	5.6	0.2	0.3	0.7	0.4
$\mathcal{B}(B \to D^* \ell \nu)$	0.7	0.3	0.2	0.3	0.4	0.3	0.3	0.5	0.4	0.3	0.5	5.7	0.3	0.3	0.7	0.4
$\mathcal{B}(B \to D^{**} \ell \nu)$	0.7	0.3	0.3	0.5	0.5	0.3	0.8	0.6	1.1	0.7	0.7	5.8	0.3	0.3	0.9	0.4
Nonresonant $b \to c \ell \nu$ BF	0.6	0.2	0.2	0.1	0.2	0.2	0.2	0.5	0.3	0.3	0.3	5.6	0.2	0.2	0.7	0.3
$B \to D \ell \nu$ FF	0.5	0.2	0.3	0.1	0.2	0.1	0.2	0.4	0.4	0.3	0.4	5.7	0.2	0.2	0.7	0.3
$B \to D^* \ell \nu$ FF	0.6	0.2	0.2	0.4	0.2	1.0	0.6	1.9	0.4	0.7	1.1	6.9	0.2	0.3	1.0	0.5
$\Upsilon(4S) \to B^0 \bar{B}^0$ BF	1.5	1.7	1.2	1.3	1.3	1.2	1.5	1.2	1.4	1.4	1.0	5.8	1.3	1.4	1.2	1.3
Secondary lepton	4.3	3.2	2.1	1.2	1.7	0.5	1.2	0.5	0.5	0.9	3.7	5.8	1.0	0.9	1.2	0.9
Final state radiation	0.3	1.3	0.8	2.2	0.3	1.4	1.2	1.3	1.4	1.6	0.8	3.4	1.0	1.1	1.5	1.2
B counting	1.1	1.1	1.1	1.1	1.1	1.1	1.1	1.1	1.1	1.1	1.1	1.1	1.1	1.1	1.1	1.1
Fit bias	0.1	0.3	0.4	0.1	0.1	0.4	0.4	0.7	0.1	1.0	2.0	30.8	0.2	0.0	1.8	0.4
Signal MC stat error	1.3	1.6	1.4	1.6	1.4	1.5	1.4	1.4	1.3	1.4	1.2	2.5	0.6	0.4	0.6	0.3
Total systematic error	12.9	6.4	6.0	4.9	5.0	5.9	5.6	7.0	7.8	6.3	10.0	61.6	4.4	4.6	8.3	5.2
Total statistical error	14.7	11.9	9.0	9.3	9.4	9.4	10.8	12.5	12.8	12.8	17.6	56.7	3.9	3.7	7.6	3.5
Total error	19.6	13.5	10.8	10.5	10.7	11.1	12.1	14.3	15.0	14.3	20.3	83.8	5.9	5.9	11.3	6.3

of q^2 and three columns for various ranges of q^2, as well as the last column for the global result. In row 1, ''Fitted yield,'' we give the raw fitted yield as the number of events. In row 2, ''Yield statistical error,'' we give the statistical uncertainty in % for each fitted yield. In row 3, ''Efficiency,'' we give the efficiency in % attached to each yield. In row 4, ''Efficiency (without FSR),'' we give the efficiency in %, modified to remove the FSR effect. In row 5, ''Unfolded yield,'' we give the yields from row 1 unfolded to give the true values of the yields in each bin, expressed as the number of events. In row 6, ''$\Delta\mathcal{B}$,'' we give the values of the partial BFs computed as usual using the true (unfolded) yields and the efficiencies with FSR. In row 7, ''$\Delta\mathcal{B}$ (without FSR),'' we give the values of the partial BFs computed as usual using the true (unfolded) yields and the efficiencies modified to remove the FSR

TABLE IX. $B^+ \to \eta^{(\prime)} \ell^+ \nu$ yields, efficiencies (%), $\Delta\mathcal{B}$ (10^{-7}), and their relative uncertainties (%).

Decay mode	$\eta'\ell^+\nu$	$\eta\ell^+\nu$ (3π)	$\eta\ell^+\nu$ ($\gamma\gamma$)				$\eta\ell^+\nu$ (3π and $\gamma\gamma$ combined)			
q^2 bins (GeV^2)	Total	Total	0–4	4–8	8–16	Total	0–4	4–8	8–16	Total
Fitted yield	141.0	244.8	279.9	216.8	146.7	643.4	303.9	331.5	252.5	887.9
Yield statistical error	32.8	25.6	13.9	17.2	33.9	12.0	14.1	14.2	26.6	11.0
Efficiency	0.61	0.59	2.01	2.55	1.42	...	2.53	3.41	1.94	...
Unfolded yield	141.0	244.8	299.1	210.9	133.3	643.4	319.3	334.8	233.9	887.9
$\Delta\mathcal{B}$	242.5	431.5	155.3	86.3	97.7	339.3	131.8	102.6	126.2	360.6
Tracking efficiency	5.2	4.1	3.2	2.4	14.6	2.6	2.1	2.0	11.1	2.8
Photon efficiency	5.6	3.1	10.1	4.3	27.4	7.0	8.0	3.8	9.0	5.7
K_L^0 efficiency	2.5	0.7	8.6	2.9	27.2	3.2	1.0	0.5	2.2	0.6
K_L^0 production spectrum	2.7	1.4	4.7	1.5	16.2	2.5	0.8	0.5	2.3	1.0
K_L^0 energy	1.1	1.4	0.6	0.5	2.5	0.9	0.6	0.4	2.3	1.0
ℓ identification	2.0	1.8	0.1	2.7	3.9	1.8	0.2	1.9	3.4	1.8
π identification	0.6	0.5	...	...	...	...	0.1	0.2	0.5	0.3
Bremsstrahlung	0.5	0.2	1.6	2.7	22.2	8.0	0.3	0.7	12.3	4.2
Continuum yield	4.9	1.1	...	...	...	...	...	...	...	...
q^2 continuum shape	5.2	2.6	2.6	1.5	4.5	0.5	2.4	0.7	2.8	0.3
$\mathcal{B}(B^0 \to \pi^- \ell^+ \nu)$	0.0	0.1	0.0	0.0	0.1	0.0	0.0	0.0	0.1	0.0
$\mathcal{B}(B^+ \to \pi^0 \ell^+ \nu)$	0.2	0.0	0.4	0.9	5.2	1.9	0.3	0.6	2.9	1.3
$\mathcal{B}(B^+ \to \eta^{(\prime)} \ell^+ \nu)$	0.4	0.4	0.0	0.1	0.8	0.2	0.1	0.1	1.0	0.4
$\mathcal{B}(B^0 \to \rho^- \ell^+ \nu)$	0.3	0.5	0.1	1.1	6.9	2.3	0.1	0.6	4.2	1.7
$\mathcal{B}(B^+ \to \rho^0 \ell^+ \nu)$	0.0	0.3	0.1	0.1	0.5	0.1	0.0	0.1	0.8	0.2
$\mathcal{B}(B^+ \to \omega \ell^+ \nu)$	0.8	1.1	0.1	0.2	2.6	0.8	0.1	0.1	2.6	0.9
Nonresonant $b \to u \ell \nu$ BF	2.3	3.5	0.4	0.9	9.5	3.1	0.5	0.6	8.6	3.4
η BF	3.1	1.2	0.5	0.7	0.7	0.6	0.5	0.6	0.7	0.5
SF parameters	4.3	6.3	1.4	2.7	16.8	6.1	1.5	2.5	14.3	6.2
$B \to \rho \ell \nu$ FF	0.1	0.7	0.1	2.3	1.7	0.9	0.1	1.5	0.9	0.5
$B^+ \to \eta^{(\prime)} \ell^+ \nu$ FF	1.1	1.0	0.1	0.1	1.4	0.4	0.1	0.1	1.5	0.6
Other scalar FF	2.9	4.2	7.7	1.4	0.1	3.2	0.7	0.1	0.0	0.2
$B \to \omega \ell \nu$ FF	1.2	2.1	0.1	0.5	2.8	0.7	0.1	0.4	3.9	1.3
$\mathcal{B}(B \to D \ell \nu)$	1.6	0.7	0.3	0.7	0.6	0.3	0.3	0.7	0.7	0.4
$\mathcal{B}(B \to D^* \ell \nu)$	0.3	0.4	0.1	0.8	1.2	0.4	0.1	0.7	1.0	0.4
$\mathcal{B}(B \to D^{**} \ell \nu)$	2.0	1.2	0.6	0.9	2.5	0.7	0.6	0.7	2.6	0.9
Nonresonant $b \to c \ell \nu$ BF	0.1	0.1	0.2	0.1	0.8	0.2	0.3	0.1	0.4	0.2
$B \to D \ell \nu$ FF	0.1	0.3	0.1	0.1	0.5	0.2	0.1	0.1	0.7	0.3
$B \to D^* \ell \nu$ FF	0.6	0.9	0.5	0.9	1.3	0.4	0.5	1.2	1.2	0.4
$\mathcal{B}(\Upsilon(4S) \to B^0 \bar{B}^0)$	1.1	1.2	1.4	1.1	0.9	1.2	1.4	1.2	1.0	1.2
Secondary lepton	4.2	5.0	1.3	0.7	9.1	2.1	1.2	1.6	9.3	3.0
B counting	1.1	1.1	1.1	1.1	1.1	1.1	1.1	1.1	1.1	1.1
Signal MC stat error	1.2	1.1	1.4	1.6	1.2	0.7	1.3	1.3	1.0	0.5
Total systematic error	14.3	12.4	17.0	8.7	55.4	14.1	9.3	6.6	28.7	11.6
Total statistical error	32.8	25.6	14.6	21.0	39.3	13.7	15.2	16.6	30.3	12.5
Total error	35.8	28.4	22.4	22.7	67.9	19.6	17.8	17.8	41.8	17.0

TABLE X. Correlation matrix of the partial $\Delta\mathcal{B}(B^+ \to \eta\ell^+\nu, q^2)$ statistical and systematic uncertainties.

	Statistical			Systematic		
q^2 bins (GeV^2)	0–4	4–8	8–16	0–4	4–8	8–16
0–4	1.00	−0.08	0.00	1.00	0.36	0.05
4–8	−0.08	1.00	−0.06	0.36	1.00	0.29
8–16	0.00	−0.06	1.00	0.05	0.29	1.00

TABLE XI. Correlation matrix of the partial $\Delta\mathcal{B}(B^0 \to \pi^-\ell^+\nu, q^2)$ statistical uncertainties.

q^2 bins (GeV^2)	0–2	2–4	4–6	6–8	8–10	10–12	12–14	14–16	16–18	18–20	20–22	22–26.4
0–2	1.00	−0.16	0.17	0.02	−0.02	0.03	0.01	0.04	0.05	0.02	0.04	−0.00
2–4	−0.16	1.00	−0.32	0.11	0.00	−0.00	−0.01	0.01	0.01	−0.00	0.00	−0.00
4–6	0.17	−0.32	1.00	−0.30	0.15	0.02	0.06	0.06	0.07	0.00	0.01	0.01
6–8	0.02	0.11	−0.30	1.00	−0.22	0.13	0.07	0.06	0.07	0.00	0.00	0.02
8–10	−0.02	0.00	0.15	−0.22	1.00	−0.22	0.16	0.05	0.08	0.01	−0.00	0.02
10–12	0.03	−0.00	0.02	0.13	−0.22	1.00	−0.15	0.10	0.07	−0.01	0.02	0.00
12–14	0.01	−0.01	0.06	0.07	0.16	−0.15	1.00	−0.16	0.13	−0.01	0.05	−0.00
14–16	0.04	0.01	0.06	0.06	0.05	0.10	−0.16	1.00	−0.01	0.01	−0.02	−0.02
16–18	0.05	0.01	0.07	0.07	0.08	0.07	0.13	−0.01	1.00	−0.17	0.09	−0.08
18–20	0.02	−0.00	0.00	0.00	0.01	−0.01	−0.01	0.01	−0.17	1.00	0.05	−0.05
20–22	0.04	0.00	0.01	0.00	−0.00	0.02	0.05	−0.02	0.09	0.05	1.00	−0.35
22–26.4	−0.00	−0.00	0.01	0.02	0.02	0.00	−0.00	−0.02	−0.08	−0.05	−0.35	1.00

TABLE XII. Correlation matrix of the partial $\Delta\mathcal{B}(B^0 \to \pi^-\ell^+\nu, q^2)$ systematic uncertainties.

q^2 bins (GeV^2)	0–2	2–4	4–6	6–8	8–10	10–12	12–14	14–16	16–18	18–20	20–22	22–26.4
0–2	1.00	−0.45	0.37	0.30	0.59	0.47	0.54	0.38	0.39	0.03	0.44	0.34
2–4	−0.45	1.00	−0.24	0.03	−0.27	−0.09	−0.17	−0.19	−0.37	0.36	−0.37	−0.02
4–6	0.37	−0.24	1.00	0.78	0.83	0.76	0.67	0.68	0.52	0.31	0.71	0.42
6–8	0.30	0.03	0.78	1.00	0.71	0.74	0.65	0.63	0.46	0.47	0.53	0.32
8–10	0.59	−0.27	0.83	0.71	1.00	0.74	0.71	0.70	0.50	0.35	0.66	0.38
10–12	0.47	−0.09	0.76	0.74	0.74	1.00	0.74	0.80	0.61	0.36	0.61	0.38
12–14	0.54	−0.17	0.67	0.65	0.71	0.74	1.00	0.69	0.73	0.29	0.56	0.33
14–16	0.38	−0.19	0.68	0.63	0.70	0.80	0.69	1.00	0.71	0.34	0.65	0.36
16–18	0.39	−0.37	0.52	0.46	0.50	0.61	0.73	0.71	1.00	−0.03	0.62	0.22
18–20	0.03	0.36	0.31	0.47	0.35	0.36	0.29	0.34	−0.03	1.00	−0.02	0.18
20–22	0.44	−0.37	0.71	0.53	0.66	0.61	0.56	0.65	0.62	−0.02	1.00	0.52
22–26.4	0.34	−0.02	0.42	0.32	0.38	0.38	0.33	0.36	0.22	0.18	0.52	1.00

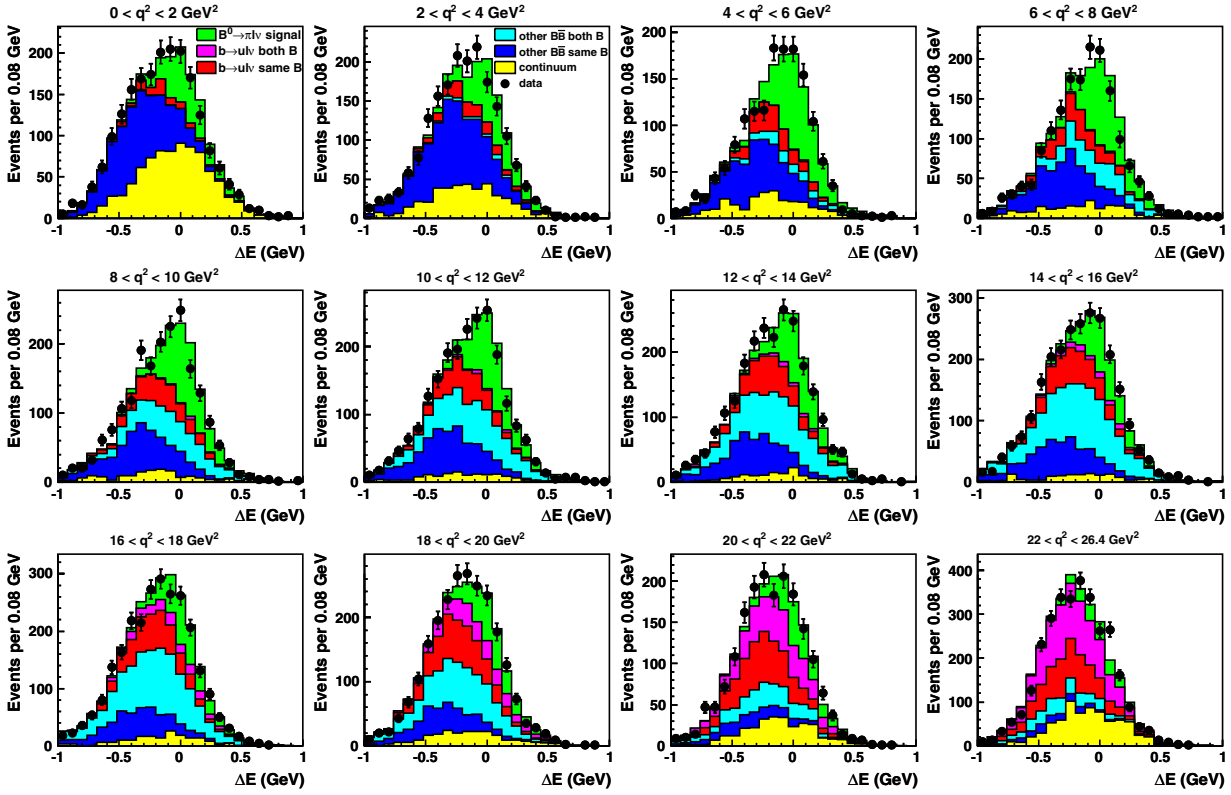

FIG. 8 (color online). ΔE yield fit projections in the signal-enhanced region, with $m_{ES} > 5.2675$ GeV, obtained in 12 q^2 bins from the fit to the experimental data for $B^0 \to \pi^- \ell^+ \nu$ decays. The fit was done using the full ΔE-m_{ES} fit region.

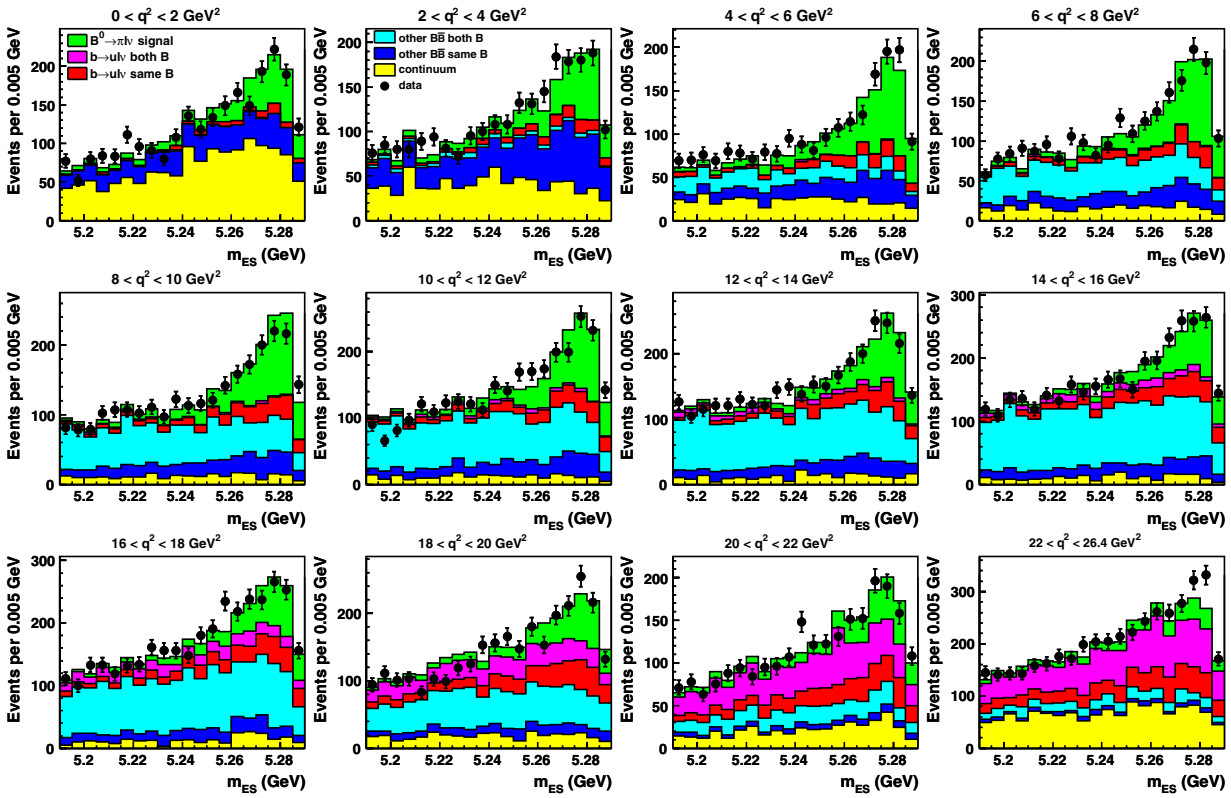

FIG. 9 (color online). m_{ES} yield fit projections in the signal-enhanced region, with $-0.16 < \Delta E < 0.2$ GeV, obtained in 12 q^2 bins from the fit to the experimental data for $B^0 \to \pi^- \ell^+ \nu$ decays. The fit was done using the full ΔE-m_{ES} fit region.

effect. In rows 8–39, we give the contributions in % to the relative systematic uncertainties for each value of $\Delta\mathcal{B}$ as a function of q^2. In row 40, ''Signal MC statistical error,'' we give the statistical uncertainty due to the number of MC signal events. In row 41, ''Total systematic error,'' we give the total systematic uncertainty in % for each value of $\Delta\mathcal{B}$, obtained as the sum in quadrature of all the systematic uncertainties in each column. In row 42, ''Total statistical error,'' we give the statistical uncertainty in % for each value of $\Delta\mathcal{B}$ obtained from propagating the statistical uncertainties on the raw fitted yields, following the unfolding process and taking into account the efficiencies. In row 43, ''Total error,'' we first give the total uncertainty in % for each value of $\Delta\mathcal{B}$, obtained as the sum in quadrature of the total systematic error and the total statistical error. We then give, in the last four columns, the total uncertainties in % for each range of q^2, obtained as the sum in quadrature of the total errors for the appropriate number of q^2 bins. A similar description applies to Table IX.

In our analysis, we compute the covariance matrix for each source of uncertainty, and use these matrices to calculate the uncertainties on the total BFs. The correlation matrices for the total statistical and systematic uncertainties are given in Table X for the $B^+ \to \eta\ell^+\nu$ yields and in Tables XI and XII for the $B^0 \to \pi^-\ell^+\nu$ yields, respectively. Finally, detailed ΔE and m_{ES} fit projections in each q^2 bin are also shown in Figs. 8 and 9, respectively, for the $B^0 \to \pi^-\ell^+\nu$ decays.

[1] M. Kobayashi and T. Maskawa, Prog. Theor. Phys. **49**, 652 (1973).
[2] E. Gulez *et al.* (HPQCD Collaboration), Phys. Rev. D **73**, 074502 (2006); **75**, 119906 (2007).
[3] C. Bernard *et al.* (FNAL/MILC Collaboration), Phys. Rev. D **80**, 034026 (2009); R. Van de Water (private communication).
[4] G. Duplancic *et al.*, J. High Energy Phys. 04 (2008) 014; A. Khodjamirian (private communication).
[5] P. Ball and G. W. Jones, J. High Energy Phys. 08 (2007) 025.
[6] Charge conjugate decays and $\ell = e$ or μ are implied throughout this paper.
[7] B. Aubert *et al.* (*BABAR* Collaboration), Phys. Rev. Lett. **98**, 091801 (2007).
[8] K. Nakamura *et al.* (Particle Data Group), J. Phys. G **37**, 075021 (2010); see, in particular, the section ''Determination of $|V_{cb}|$ and $|V_{ub}|$.''
[9] S. B. Athar *et al.* (CLEO Collaboration), Phys. Rev. D **68**, 072003 (2003); D. M. Asner *et al.* (CLEO Collaboration), Phys. Rev. D **76**, 012007 (2007); N. E. Adam *et al.*, Phys. Rev. Lett. **99**, 041802 (2007).
[10] B. Aubert *et al.* (*BABAR* Collaboration), Phys. Rev. Lett. **97**, 211801 (2006).
[11] T. Hokuue *et al.* (Belle Collaboration), Phys. Lett. B **648**, 139 (2007).
[12] B. Aubert *et al.* (*BABAR* Collaboration), Phys. Rev. D **79**, 052011 (2009).
[13] B. Aubert *et al.* (*BABAR* Collaboration), Phys. Rev. Lett. **101**, 081801 (2008).
[14] P. del Amo Sanchez *et al.* (*BABAR* Collaboration), Phys. Rev. D **83**, 032007 (2011).
[15] B. Aubert *et al.* (*BABAR* Collaboration), Nucl. Instrum. Methods Phys. Res., Sect. A **479**, 1 (2002).
[16] D. Côté *et al.*, Eur. Phys. J. C **38**, 105 (2004).
[17] D. Becirevic and A. B. Kaidalov, Phys. Lett. B **478**, 417 (2000).
[18] C. Amsler *et al.* (Particle Data Group), Phys. Lett. B **667**, 1 (2008).
[19] B. Aubert *et al.* (*BABAR* Collaboration), Phys. Rev. D **74**, 092004 (2006).
[20] G. Cowan, *Statistical Data Analysis* (Oxford University Press, New York, 1998), Chap. 11.
[21] G. C. Fox and S. Wolfram, Phys. Rev. Lett. **41**, 1581 (1978).
[22] B. Aubert *et al.* (*BABAR* Collaboration), Phys. Rev. D **67**, 031101 (2003).
[23] R. J. Barlow and C. Beeston, Comput. Phys. Commun. **77**, 219 (1993).
[24] O. L. Buchmüller and H. U. Flächer, Phys. Rev. D **73**, 073008 (2006).
[25] E. Richter-Was *et al.*, Phys. Lett. B **303**, 163 (1993).
[26] E. Barberio and Z. Was, Comput. Phys. Commun. **79**, 291 (1994).
[27] Y. Zhu, arXiv:0812.2708v1.
[28] C. G. Boyd and M. J. Savage, Phys. Rev. D **56**, 303 (1997).
[29] T. Becher and R. J. Hill, Phys. Lett. B **633**, 61 (2006).
[30] H. Ha *et al.* (Belle Collaboration), arXiv:1012.0090v4 [Phys. Rev. D (to be published)].